Best Available
Copy
for all Pictures

AD-784 433

HOLOGRAPHIC STUDY OF ROCK SPECIMENS
UNDER UNIAXIAL AND TRIAXIAL LOADS

J. L. Schmidt, et al

TRW Systems Group

Prepared for:

Defence Nuclear Agency
Defence Advanced Research Projects Agency

9 August 1974

AD 784 433

REPORT DOCUMENTATION PAGE		READ INSTRUCTIONS BEFORE COMPLETING FORM
1 REPORT NUMBER DNA 3344F	2. GOVT ACCESSION NO.	3. RECIPIENT'S CATALOG NUMBER
4 TITLE (and Subtitle) Holographic Study of Rock Specimens Under Uniaxial and Triaxial Loads		5 TYPE OF REPORT & PERIOD COVERED Final Report 10 July 1972 - 12 Dec. 1973
		6 PERFORMING ORG. REPORT NUMBER
7 AUTHOR(s) J. L. Schmidt T. J. Ahrens, Consultant J. D. O'Keefe		8 CONTRACT OR GRANT NUMBER(s) DNA 01-71-C-0100
9 PERFORMING ORGANIZATION NAME AND ADDRESS Advanced Technology Staff, Space Vehicles Div. TRW Systems Group One Space Park, Redondo Beach, CA 90278		10 PROGRAM ELEMENT, PROJECT, TASK AREA & WORK UNIT NUMBERS ARPA M06FAZL468,01
11 CONTROLLING OFFICE NAME AND ADDRESS Director Defense Nuclear Agency Washington, D.C. 20305		12 REPORT DATE 9 August 1974
		13 NUMBER OF PAGES 59
14 MONITORING AGENCY NAME & ADDRESS(if different from Controlling Office)		15 SECURITY CLASS (of this report) Unclassified
		15a DECLASSIFICATION DOWNGRADING SCHEDULE N/A

16 DISTRIBUTION STATEMENT (of this Report)

Approved for public release; distribution unlimited.

17 DISTRIBUTION STATEMENT (of the abstract entered in Block 20, if different from Report)

18 SUPPLEMENTARY NOTES

This work was supported by the Advanced Research Projects Agency under
ARPA Order No. 1468, Subtask ZL468.

19 KEY WORDS (Continue on reverse side if necessary and identify by block number)

Holography
Holographic Interferometry
Rock Mechanics
Strain
Triaxial Loading

Uniaxial Loading

20 ABSTRACT (Continue on reverse side if necessary and identify by block number)

Double-exposure holographic interferometry was used to measure the radial
and axial displacement profiles over the surface of cylindrical specimens of
rock placed under uniaxial and triaxial loads. The rock specimens tested were
Mixed Company Sandstone and Lithographic Limestone. The axial loads used in
the tests were in the range of 1000 psi to 1600 psi. The hydrostatic pressure
for the triaxial test was 4000 psi. Strain distributions were calculated and
comparisons were made between the measured total axial strain on the Mixed
Company Sandstone specimens and results obtained using conventional strain

DD FORM 1 JAN 73 1473   EDITION OF 1 NOV 65 IS OBSOLETE   I.

gauge techniques. A special test pressure vessel was built with a viewing port to accommodate the use of holographic interferometry to measure the surface response of the sandstone specimen during the triaxial test.

TRW
SYSTEMS GROUP

TABLE OF CONTENTS

TRW SYSTEMS GROUP

1.0 INTRODUCTION AND SUMMARY

The work described herein was accomplished under contract DASA01-71-C-0100, "Measurements of the Response of Geologic Materials." In two previous phases TRW developed advanced optical techniques, laser holographic interferometry and moire interferometry for use in measuring the stress wave propagation response of granite rods. In this phase of the contract the technique of double exposure holographic interferometry was used to measure the strain response of cylindrical rock specimens subjected to uniaxial and triaxial loads.

Conventional uniaxial and triaxial tests use strain gauges which measure only the total axial strain or extension of the cylinder over its total length and the peak radial expansion during the tests. Holographic interferometry enables one to measure the full field axial and radial displacement profile and thus the strain distribution over the entire surface of the specimen. Holographic interferometry is less amenable to bulk testing however, because the interferograms are recorded in relatively small loading steps.

The purpose of this program was to demonstrate the potential of holographic interferometry in uniaxial and triaxial tests for measuring the strain distributions along the axis of two cylindrical rock specimens. In the course of the program it was necessary to develop a special pressure vessel for the triaxial tests and determine the feasibility of obtaining holographic interferograms through the pressure vessel optics during a triaxial load test.

The use of a glass viewing port for performing the holography on the specimen inside of the pressure vessel did not pose a problem for this work. A commercial boiler sight glass window was used for working pressures up to 5000 psi. Windows have been designed and used for pressures up to several kilobars (Ref. 1). The transparency of the protective membrane for the specimen in a triaxial test was solved by encapsulating the specimen and two steel caps in shrinkable polyurethane tubing.

1

Obtaining accurate strain measurements in a triaxial pressure
vessel using holographic interferometry depends on the elimination
of small changes that can occur in the pressure vessel optics during
axial loading of the specimen. Holographic interferometry measures
the displacement of a point on the specimen by recording on film via
fringe patterns the change in the total optical path length between
the laser source and the film emulsion. However, these optical path
length changes can also include changes in index of refraction of the
media through which the laser light must pass. In the case of triaxial
tests, this includes the viewing port window, changes in the pressure
of the working fluid and distortions of the transparent membrane
enclosing the specimen.

Stored-beam holography was used in conjunction with analytic
studies to determine the effect of these small changes in the working
fluid pressure on the holography. It was found necessary to maintain
the pressure of the fluid to within less than 1% during a test to
insure that no fringes were formed in the holographic image due solely
to changes in the index of refraction of the working fluid.

In the series of tests performed, holographic interferometry was
used first to measure the radial and axial displacement profiles along the
axis of Mixed Company Sandstone and Lithographic limestone in uniaxial
tests. The specimen sizes were 1/2 inch by 1-1/2 inches. Load steps
of 350 psi and 1000 psi were used in these tests respectively.
In addition, axial strain distributions were obtained in both of these
tests along with displacement profiles. The sandstone tests
showed a large variation in the local axial strain over the average
strain. The strain profiles, although smooth, showed a high concentration
of strain toward one end of the specimen. These types of measurements
have been shown to predict the location of failure on the specimens
(Ref. 2) when the load approached the specimen limit.

There was good agreement between the total axial strains obtained
in the Mixed Company Sandstone tests and those obtained by conventional

strain gauges. There was some uncertainty in the peak amplitude of the radial displacement profiles. This was a result of not being able to accurately account for the absolute rigid body tilt of the specimen in the data. This tilt, which was not measured independently, is simultaneously recorded in addition to the radial expansion of the specimen and must be subtracted out. For our purposes, reasonable results were achieved by assuming that the ends of the specimen did not expand during the test and that the displacements measured at the ends of the specimen represented tilt only. The rigid body tilt could be accurately measured during a test using a strain gauge or linear interferometer.

Successful interferograms of a Mixed Company Sandstone specimen surface were obtained during a triaxial test in a pressure vessel fitted with a port window. For this test the hydrostatic pressure (σ_3) was maintained at 4000 psi $\pm$ 50 psi. The axial load ($\sigma_1 - \sigma_3$) set initially to + 1000 psi was increased in load steps of 350 psi. The radial and axial displacement profiles obtained were similar to those in the uniaxial test with the axial strain showing a point of higher concentration.

2.0 HOLOGRAPHIC INTERFEROMETRY

2.1 Applications to Compressive Tests on Geologic Specimens

The work herein demonstrates the application of holographic interferometry to studying the surface of cylindrical specimens of rock subjected to axial compressive and triaxial loads. Application to a compressive test is straightforward. A photograph of such a setup is shown in Figure 1. Figure 2 shows a schematic of the basic holographic arrangement. The cylindrical specimen is loaded in the usual manner with two exceptions. First, the load structure allows for the illumination of and photographing of the specimen surface during the test. Second, the specimen is loaded in steps to allow permanent interferograms to be recorded of the surface displacements during each load step.

The recording of the interferograms and subsequent determination of the displacement fields goes as follows. The tests are carried out in a dark room since open photographic plates or film strips are used. The specimen is preloaded to a desired load. A single exposure of the specimen surface illuminated with a laser source is recorded on the two photographic plates. This constitutes the reference hologram for that load step and the first exposure of the double-exposure interferogram. The load is then increased to the desired amount and a second exposure made on the same photographic plates. The plates are then replaced with a new set for the next load step. When the test is complete, each developed set of plates contain separate interferograms for the respective load steps. These developed plates are then placed in the original setup where the reconstructed interferograms (fringed images) of the specimen can be photographed for data reduction. Two plates are used in this setup because the fringe patterns are different for each of the viewing angles. The geometry and the fringe orders for the two respective viewing angles
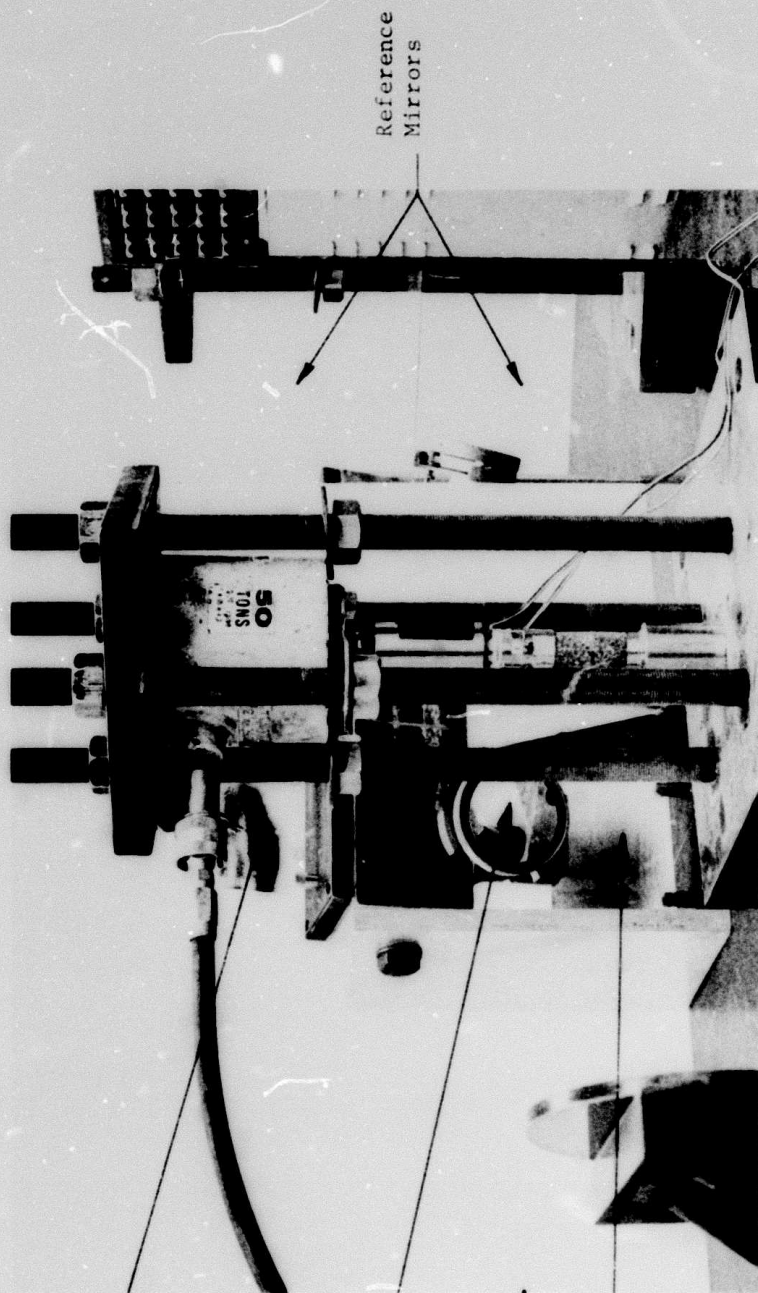
Reference
Mirrors

Upper
Hologram
(View 2)

Mirror
forming
converging
scene beam

Lower
Hologram
(View 1)

Figure 1: Photograph showing the specimen in the loading aparatus and the two glass hologram plates in the background.

5

provide two simultaneous equations from which the two displacement values at each point on the specimen can be calculated.

The magnitude of the selected load steps must be determined prior to the test, preferably by using a stored-beam setup to study the response of the specimen in real-time. If too many fringes are recorded in the double-exposure interferogram, photographing them will be difficult and data reduction more laborious. Too few fringes will not allow accurate interpolation between fringes and thus does not allow a detailed analysis of the displacement fields.
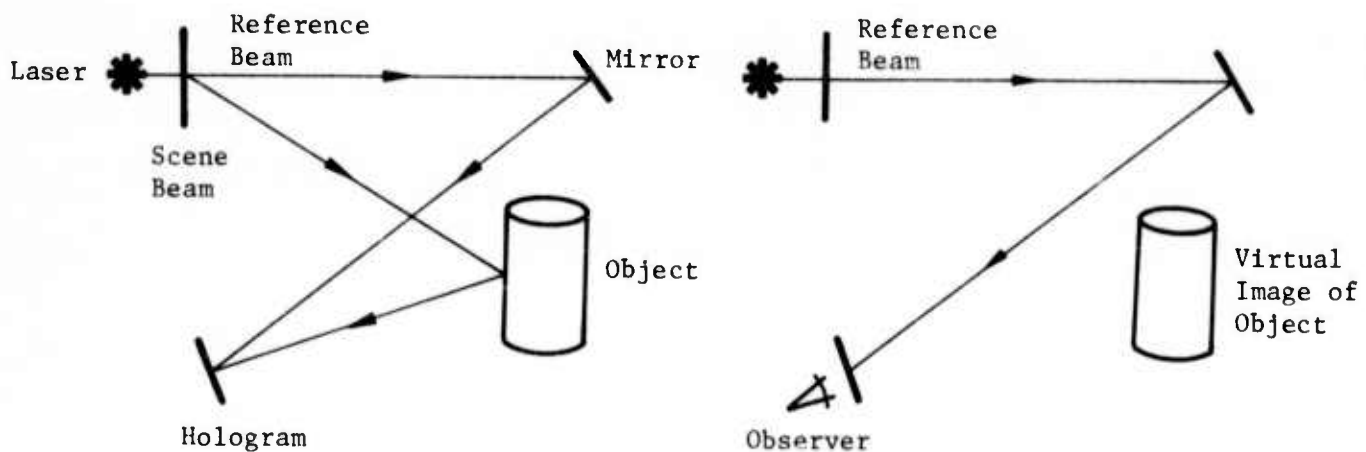
Figure 2: Left: Image recording process
Right: Image retrieval

2.2 Application to Triaxial Tests

There are two problems to overcome in applying holographic interferometry to measuring local strain fields over specimens in an enclosed triaxial test. The obvious problem is related to performing the required holographic recording operation inside or through the high pressure vessel encasing the specimen during the test. The second problem is the effect of the pressurized media surrounding the specimen and the specimen encasement membrane on the holographic recording and subsequent data reduction.

2.2.1 Pressure Vessel Design

A pressure vessel was designed with a special sight window to accommodate holographic interferometry during the test. The pressure vessel was designed for hydrostatic working pressures up to 5,000 psi. A load cell was included in the design to record axial loads up to 2.5 Kbar. A cutaway schematic of the pressure vessel is shown in Figure 3. The pressure vessel was fabricated out of a single billet of steel. Viewing and illumination of the specimen with laser light are accomplished by incorporating a rectangular sight glass in the side of the pressure vessel. For our purposes a commercially available high pressure boiler sight glass was used. The sight glass was rated at 5,000 psi working pressure. Care was taken to properly seal the sight glass. The pressure vessel is shown disassembled in Figure 4. Figure 5 shows the pressure vessel in a load configuration with the specimen in place.

2.2.2 Specimen Preparation for Holographic Triaxial Tests

When using holographic interferometry in a triaxial compressive test, the specimen's surface must be accessible to illumination and viewing during the test. Therefore, it was necessary to make a transparent protective jacket for the specimen. For our tests the specimen was prepared as shown in Figure 6. The specimen is lightly cemented between two steel caps. A transparent jacket is then bonded
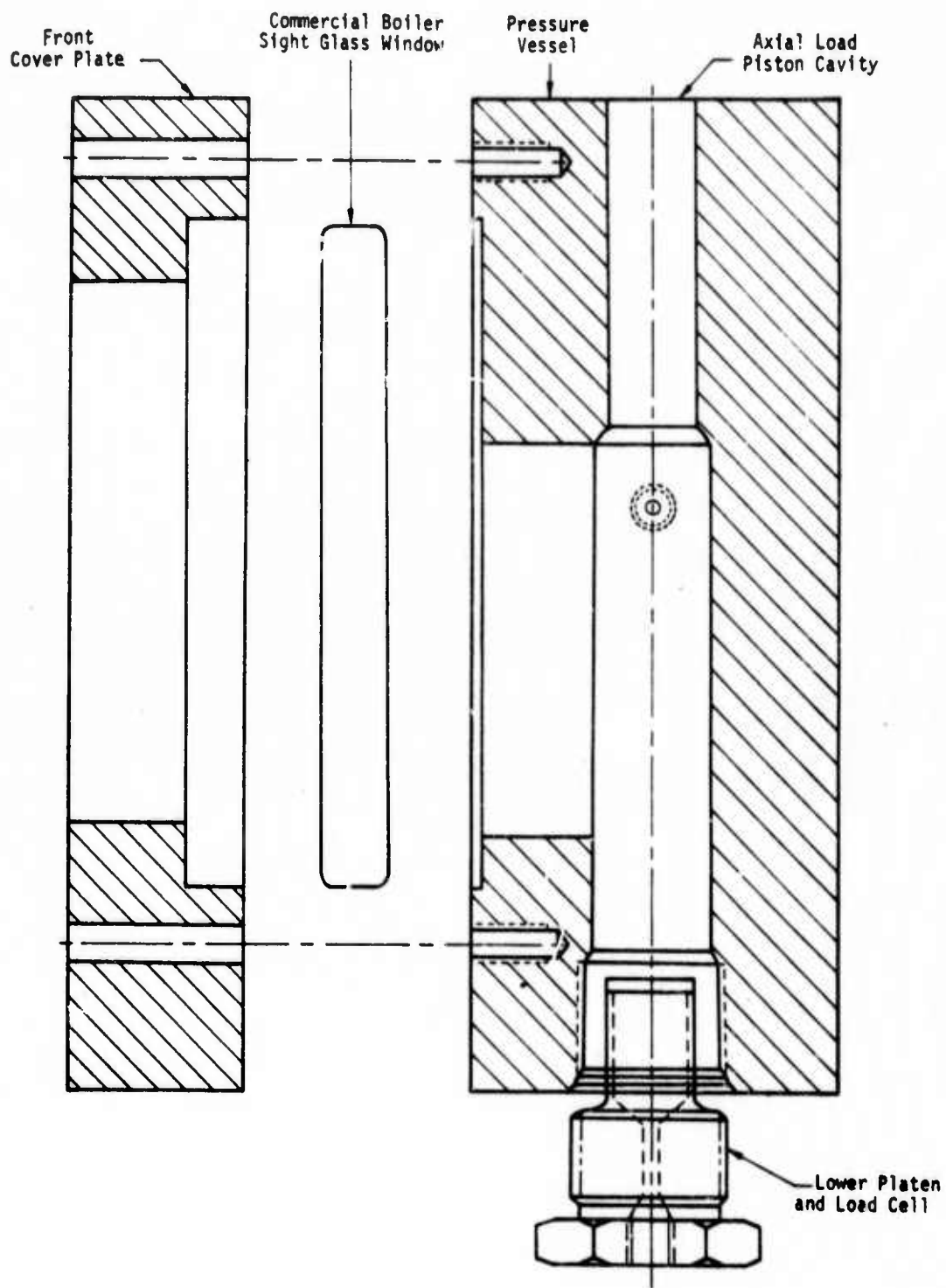
7

Figure 3: Cross section of the disassembled triaxial test pressure
vessel for use with holographic interferometry. A
commercial boiler sight glass was used as a viewing port
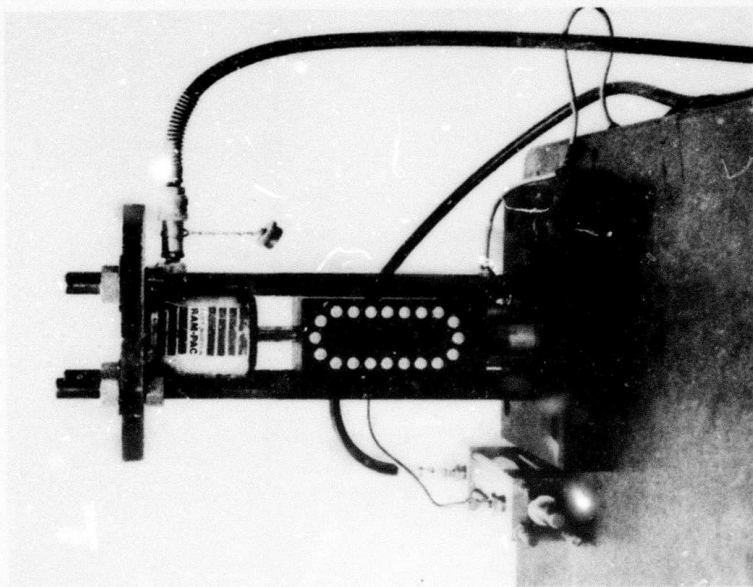for the holographic optics.

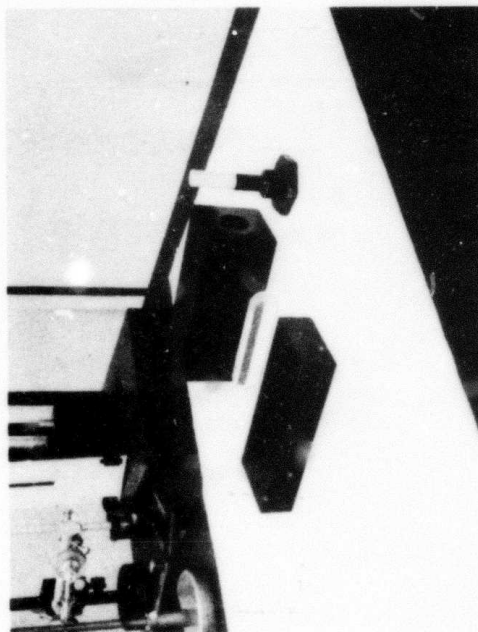Figure 5: The holographic triaxial test cell in its loading configuration.

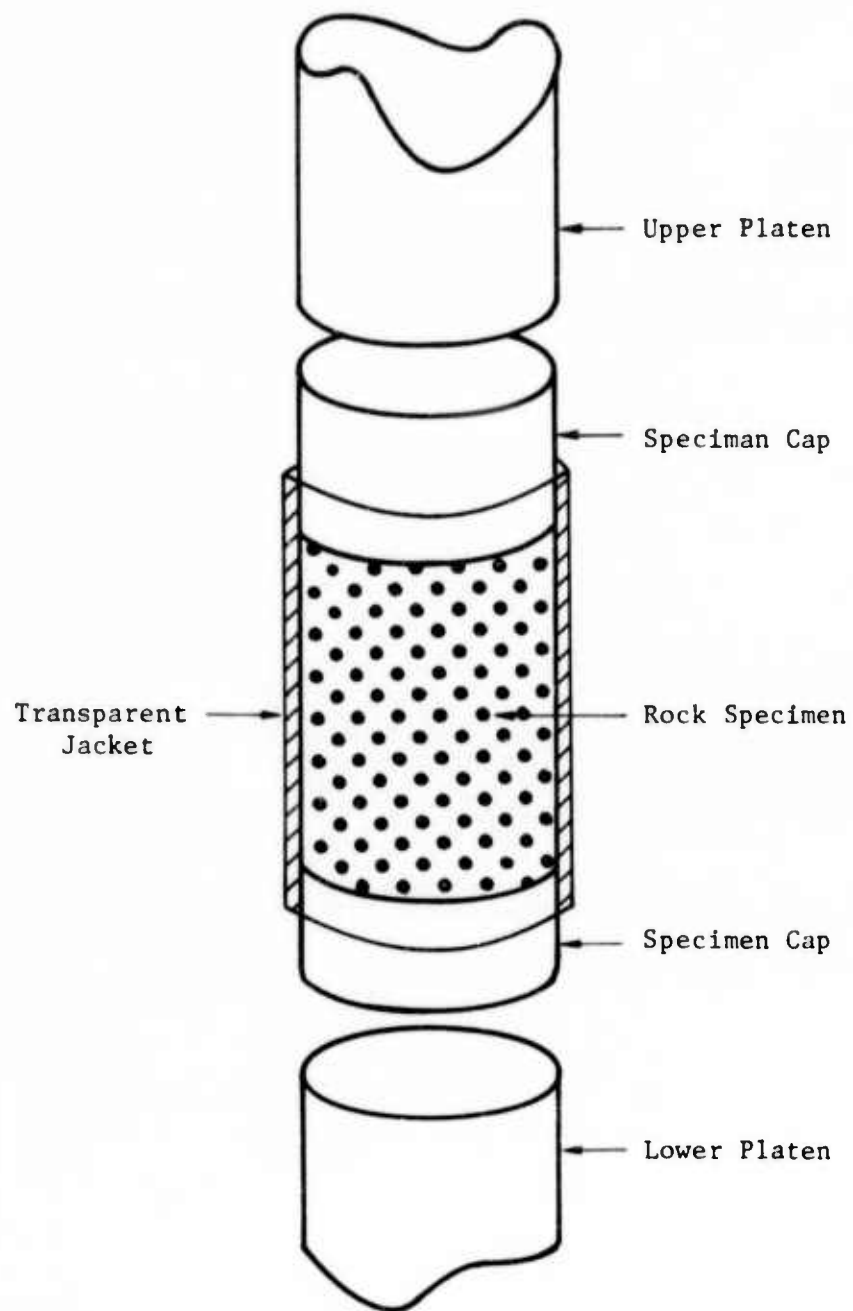Figure 4: Triaxial holographic pressure vessel disassembled.

9

Upper Platen

Speciman Cap

Transparent
Jacket

Rock Specimen

Specimen Cap

Lower Platen

Figure 6: Details of specimen preparation for holographic triaxial test.

around this core. It was found convenient to use polyurethane
shrinkable tubing. The tubing had an original diameter of approximately
3/4". The wall thickness is approximately .030 inches after shrinkage.
The ends of the plastic tubing are bonded to the end caps to prevent
the working fluid from contacting the specimen.

The transparency of the protective casing is very important. If
the surface of the plastic is roughened inside or out, this surface
will be imaged along with or instead of the specimen surface. This
will prevent or make recording of interferograms of the specimen's
surface very difficult. This was encountered when working with
sandstone specimens where the large protruding grains embedded in the
plastic and degraded its transparency.

2.2.3 Holography Through Pressurized Liquid Media

Holographic interferometry is based on the relative changes in
the phases of two coherent beams between two exposures of a hologram.
The differences in the phases or optical path lengths from one
exposure to the next give rise to interference patterns upon
reconstruction of the hologram. This interference pattern is then
converted to displacement fields by determining the changes in the
optical paths which produced the interference pattern. When making
double-exposure holograms of a specimen located inside a vessel
surrounded by a pressurized medium, there are several sources
contributing to optical path length changes other than displacement
of the specimen surface.

Considering Figure 7, the scene beam is transported through a
port window through the pressurized liquid medium and is finally
reflected off the specimen. If a double-exposure hologram is made
with this setup, no fringes will form over the reconstructed image
as long as there are no changes in optical path lengths between
exposures.

However, by simply increasing the internal pressure of the vessel
by an amount Δp between exposures, changes in optical path lengths
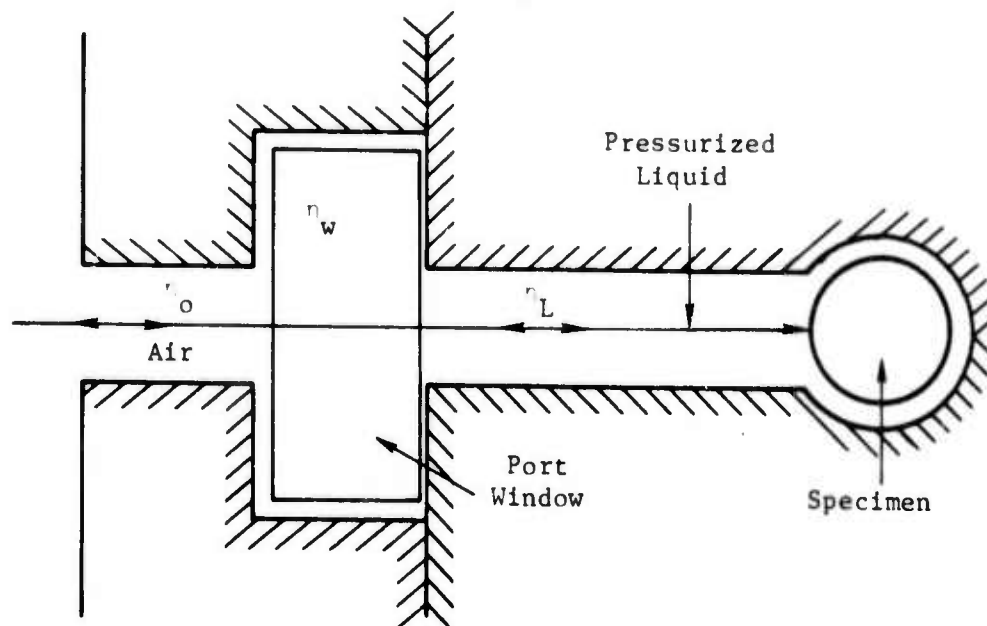
Figure 7: Schematic of holographic ray path through the viewing port of the pressure vessel.

will occur through the pressure vessel and the relative differences in phases will be recorded on film. Figure 8 shows the physical changes in path lengths of the beam which could occur as a result of increasing the pressure of the fluid between exposures.

The optical path length changes arise from three sources. The port window will be displaced outward by an amount dw giving a path length change of δ_w. The specimen will be compressed, giving a negative displacement dr of the surface and a path length change δ_s. And third, the index of refraction of the pressurized liquid (η) which is a function of pressure will change by an amount $\Delta\eta = \frac{\partial \eta}{\partial P}\bigg|_p \Delta p$ giving a path length change δ_L. The total path length change is the sum of the path length changes:

$$\Delta\delta_t = \Delta\delta_s + \Delta\delta_w + \Delta\delta_L \tag{1}$$

12

Figure 8: Optical path length changes due to an increase in the hydrostatic pressure by an amount ΔP.

The optical path length is defined as

$$\delta = \eta L \tag{2}$$

where η is the index of refraction of the medium and L is the length of the path. The change in the optical path length is the derivative

$$\Delta \delta = \eta dL + L d\eta \tag{3}$$

The changes in the physical path length dL and the change in the

index of refraction are both functions of pressure. We now use
Equations (2) and (3) to analyze each of the terms in Eq. (1). Thus,
changes in optical path length due to hydrostatic compression of the
specimen are given by

$$\Delta\delta_s = \eta dr \cos\theta \tag{4}$$

The deflection of the window gives rise to a path length change of

$$\Delta\delta_w = (\eta_w - \eta_o) \, dw_o(\theta) + (\eta_L - \eta_w) \, dw_i(\theta) \tag{5}$$

where η_o is the index of refraction of air,

η_w is the index of refraction of the window

η_L is the index of refraction of the liquid and

dw_i and dw_o are deflections of the inside and outside of
the window, respectively.

The change in the optical path length due to the change in index of
refraction of the liquid $d\eta_L$ is

$$\Delta\delta_L = Ld\eta_L \tag{6}$$

where
$$d\eta_L = \frac{\partial\eta}{\partial p}\bigg|_p \Delta p$$

Combining Equations (4), (5) and (6) we have for the total change in
the optical path length due to a change in the internal pressure
of Δp:

$$\Delta\delta_t = \eta_L \, dr \cos\theta$$

$$+ (\eta_w - \eta_o)dw_o(\theta) + (\eta_L - \eta_w)dw_i(\theta) \tag{7}$$

$$+ L(\theta) \, (\partial\eta_L/\partial p)\Delta p$$

A dark fringe will occur whenever the path length changes by an amount

$$\Delta\delta_t = \frac{\lambda(2n - 1)}{2}$$

where λ is the wavelength of the laser light and n is the fringe order. Since dr, dw and $d\eta_L$ are all functions of the pressure change Δp, the required constraint on the hydrostatic pressure to prevent fringes from forming during a test can be determined. It is necessary to keep the hydrostatic pressure constant within this constraint during a test to prevent the optical path length changes caused by changes in the hydrostatic pressure from being added onto those due solely to the axial load on the specimen.

For our purposes we determined this constraint experimentally. In Eq. (7) the first and last term will result in straight fringes being formed on the specimen parallel to the axis. The second term will result in square or elliptical fringes to be formed when changing the hydrostatic pressure between holographic exposures. Both types of fringes were observed experimentally. For pressures up to 5,000 psi no fringes were formed as long as the hydrostatic pressure was kept constant within $\pm$ 50 psi. This is easily determined using a stored-beam holographic setup.

3.0 DATA REDUCTION METHODS

In general, the conversion of the fringe patterns covering a specimen to displacement fields requires the determination of optical path length changes during the test over the complete visual field. This requires a knowledge of the geometry of the holographic setup and the labeling of fringe orders. A knowledge of the holographic optics geometry and how it can affect the calculated values of the displacement field is necessary to obtain the desired type of data. This is particularly true in the case of a triaxial test where the small viewing window places a constraint on the holographic optics geometry.

Due to the tremendous amount of data that is inherent in a single interferogram (theoretically it is possible to determine the three displacement components at each point on the specimen) it was necessary to write a computer program to reduce the interferograms to displacement fields. This computer program was based on the holographic analysis derived by Dhir and Sikora (Ref. 3). The advantage of their approach is the increased accuracy in determining the displacements when using a small field of view and the elimination of the need to know the absolute order of the fringes.

3.1 Holographic Analysis of a General Displacement Field

A general diagram of the ray paths in a holographic setup for measuring a general displacement field PP' (x,y,z) is shown in Figure 9. The points S and H represent the laser light source and viewing point through the hologram respectively. P and P' are the points on the specimen before and after displacement has occurred.

A double exposure hologram is formed by exposing the hologram first to the ray paths HPS and then to the ray paths HP'S after the object has been displaced. Upon reconstruction of the hologram, dark fringes occur whenever the phase difference between the two paths is $(2n - 1)\pi$ radians. The phase difference between the ray path SPH and SP'H is

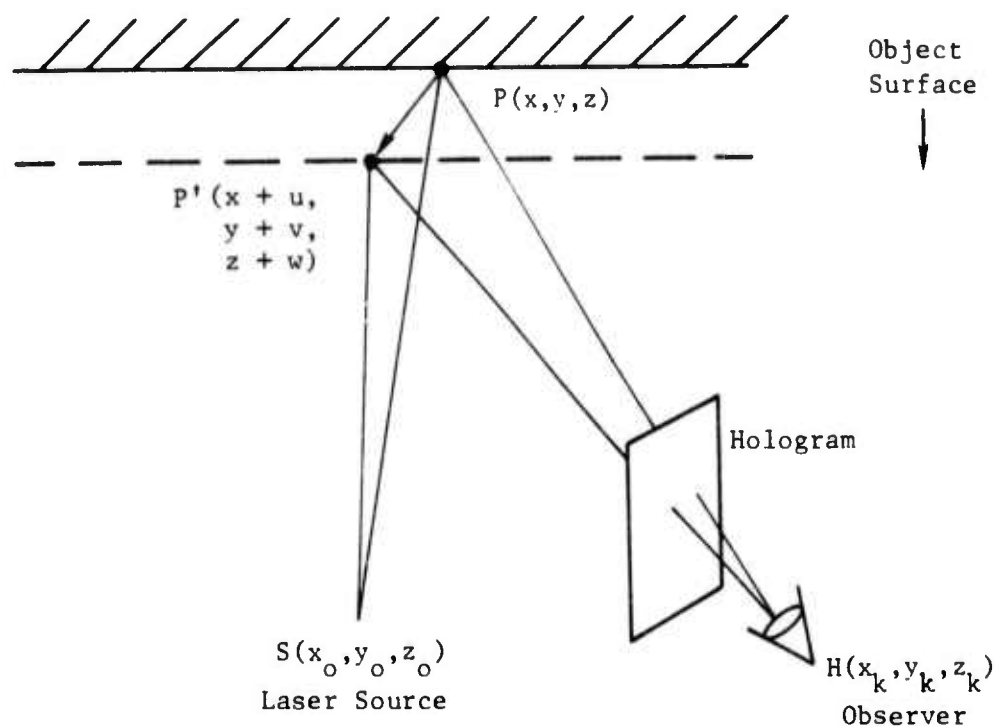$$\delta_K = \frac{2\pi}{\lambda} (SP' + P'H) - (SP + PH) \tag{1}$$

16

Figure 9: Diagram of ray path movements in a double exposure hologram where the object surface is displaced along the path PP' between exposures. H is the hologram; S is the laser source.

where

$$SP' - SP = \frac{(x - x_o)u + (y - y_o)v\ (z - z_o)w}{R_o} \tag{2}$$

and

$$HP' - HP = \frac{(x - x_K)u + (y - y_K)v + (z - z_K)w}{R_K} \tag{3}$$

R_o and R_K are the distances between the laser source and object point P_K and the distance between the object point P_K and the observation point H_K on the hologram respectively; u, v and w are the respective object displacements in the x, y and z directions. Since

$$\delta_K = (2n - 1)\pi \tag{4}$$

for dark fringes, then

$$\delta_K = \frac{2\pi}{\lambda} (A_K u + B_K v + C_K w) = (2n_K - 1)\pi \tag{5}$$

where A_K, B_K and C_K are the direction cosines given by

$$A_k = \frac{x - x_o}{R_o} + \frac{x - x_K}{R_K} \tag{6}$$

$$B_K = \frac{y - y_o}{R_o} + \frac{y - y_K}{R_K} \tag{7}$$

$$C_K = \frac{z - z_o}{R_o} + \frac{z - z_K}{R_K} \tag{8}$$

or

$$A_K u + B_K v + C_K w = (2n_K - 1)\lambda/2 \tag{9}$$

where n_K is a single point on the object corresponding to the fringe number n and observation point K on the hologram. n_K (i.e., the absolute fringe order at P_K) is not, in practice, always determinable. To overcome this problem, the fringe shift or number of fringes that traverse a point on the object is measured when shifting the observation point from one position to another on the hologram (say from K to $K + 1$). When two equations of type 9 are written for the two observation points (H_K and H_{K+1}) and subtracted they yield

$$(A_K - A_{K+1})u + (B_K - B_{K+1})v + (C_K - C_{K+1})w = (n_K - n_{K+1})\lambda \tag{10}$$

Dhir and Sikora point out that only three equations of the above type are necessary to obtain u, v and w at P(x,y,z). However, the determinant formed by the coefficients of the system of three simultaneous equations is very small due to the geometry created by the small aperture of a single holographic plate. This causes large uncertainties in the calculations of the respective displacements at

18

TRW.
SYSTEMS GROUP

P(x,y,z). Two holographic plates require a knowledge a priori of the zero order fringe. Dhir and Sikora therefore have advanced one step further in the analysis. To improve the accuracy of a single holographic plate, Dhir and Sijora show that by using a least squares approach the desired accuracy is obtained by using one more equation or viewing point than there are displacement components to be determined. Thus, to obtain u, v and w requires four photographs of the interferogram from four separate viewing directions which will give at least four equations of type (10).

3.2 The Data Reduction Process

The fringe patterns in each interferogram were photographed from four different locations through the reconstructed holographic plate or film. Reconstruction of the test holograms (photographic plates or film strips containing the interferograms) was accomplished in the same setup used for recording them. This preserves the holographic geometry required for data reduction.

The fringes in the first photo were given arbitrary fringe orders. Subsequent photos were given fringe orders according to the shift of the fringes as the camera is moved from one position to another. These photographed fringe patterns were digitized and input to the code where they are fitted with a low order polynomial for interpolation purposes.

The holographic data reduction computer code determined the fringe orders at predetermined grid points on the specimen for each of four photos. It then computed the three displacement components at these grid points using Equation (10) for each of the four photos in a least squares determination.

The accuracy of the code was demonstrated in the following test case. Fringe patterns were computed for an aluminum specimen compressed by a 3,000 pound per square inch load between exposures. The specimen dimensions were 3/4 inch diameter by 1.5 inches long. The fringe pattern along the axis for each of four viewing positions

in a simulated holographic geometry is shown in Figure 10. These fringes were put into the computer code along with the simulated holographic geometry. The theoretical axial and radial displacement fields used to generate the simulated fringe patterns are shown in Figure 11 along with the calculated values obtained from processing the fringe patterns in the computer code. Excellent agreement was obtained for both the axial and the radial displacements.

3.3 An Interferogram Recorder

To provide ease of data reduction and to eliminate the need for determining the absolute fringe orders when using two holographic plates during a test, a special film holder was built to record the holograms. By using film, the hologram length can be increased to any desired length. This allows the viewer a continuous scan of the holographic image so that the magnitude of the shift in the fringe patterns can be determined from one viewing direction to the next.

The use of film cassettes in conjunction with the film holder simplifies the recording operation during a test since the test must be carried out in darkness to expose the plates. A schematic of the film interferogram recorder is shown in Figure 12. It is shown in use in Figure 13. In actual practice the cassettes were not used as it was found easier to work with precut strips of film. However, once operating procedures are established a mechanized film cassette will be of definite assistance. The recorder was designed to take up to 105mm size film. We used Agfa Gavaert 10E75 70mm film cut into strips about 15-18 inches long.
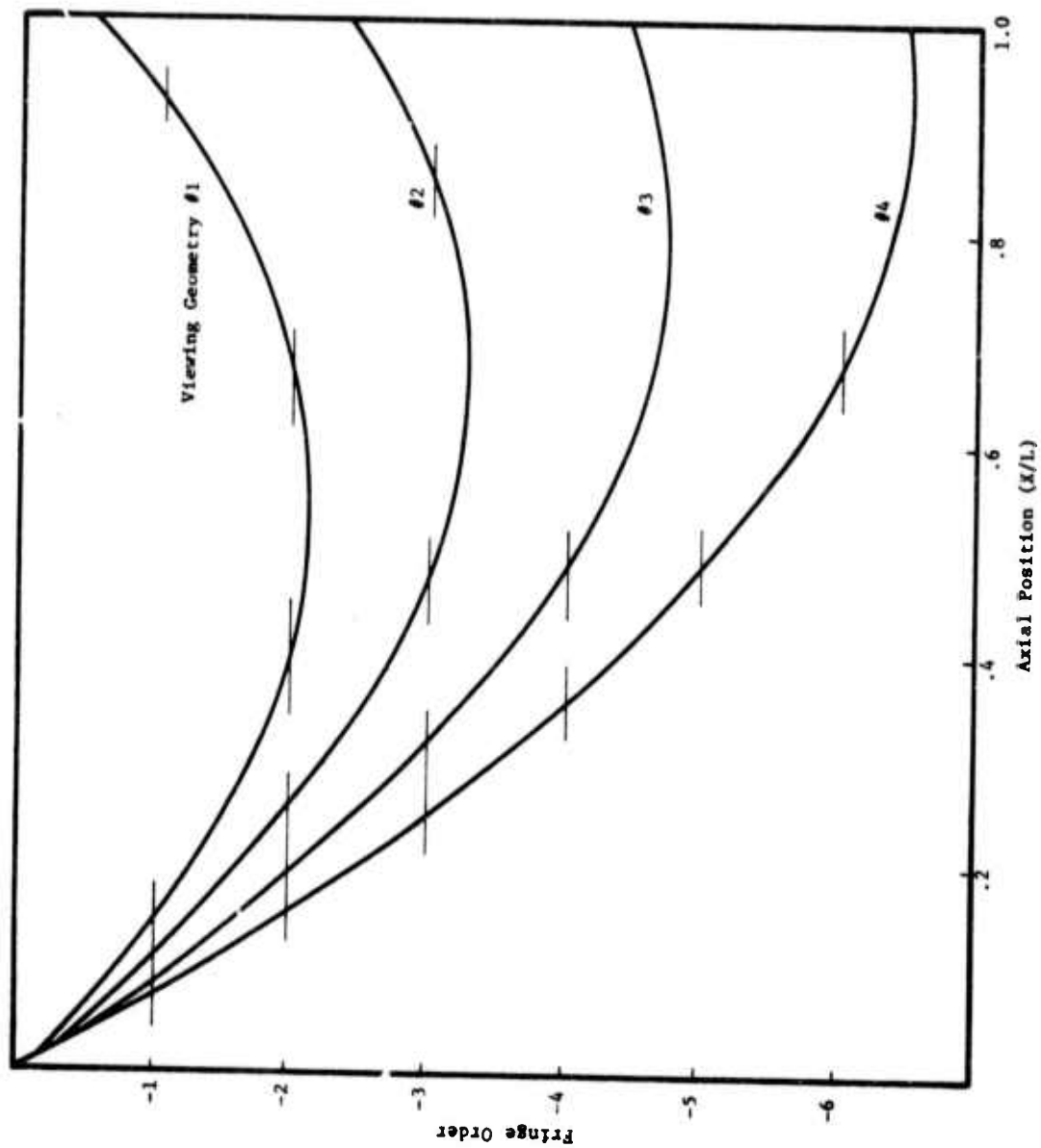
Figure 10: Theoretical fringe patterns for four viewing directions in a simulated double exposure hologram of an aluminum cylinder loaded to 3,000 psi.
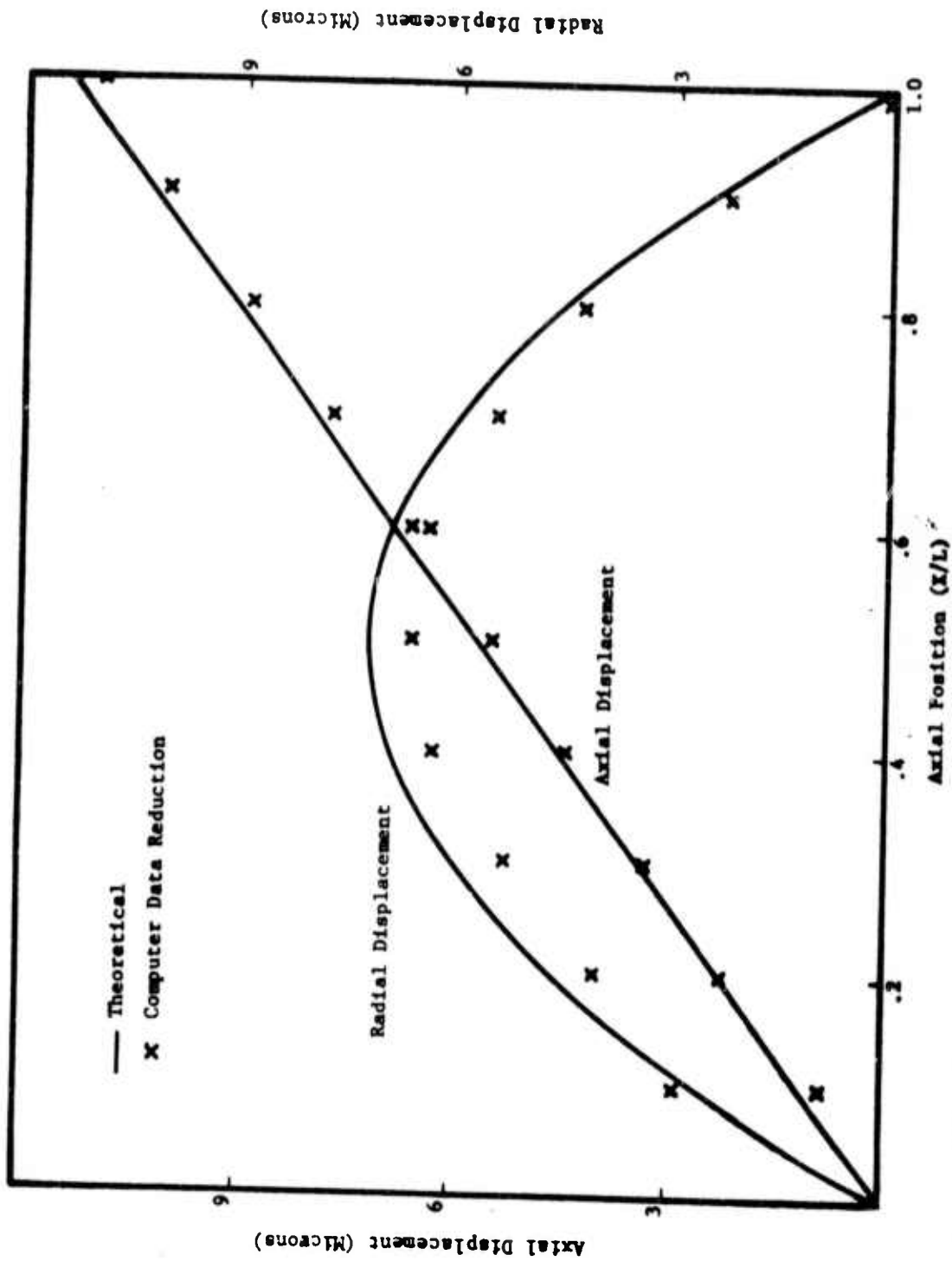
Figure 11: Theoretical axial and radial displacement profiles of aluminum cylinder loaded to 3,000 psi compared to computer data reduction of simulated fringe patterns.
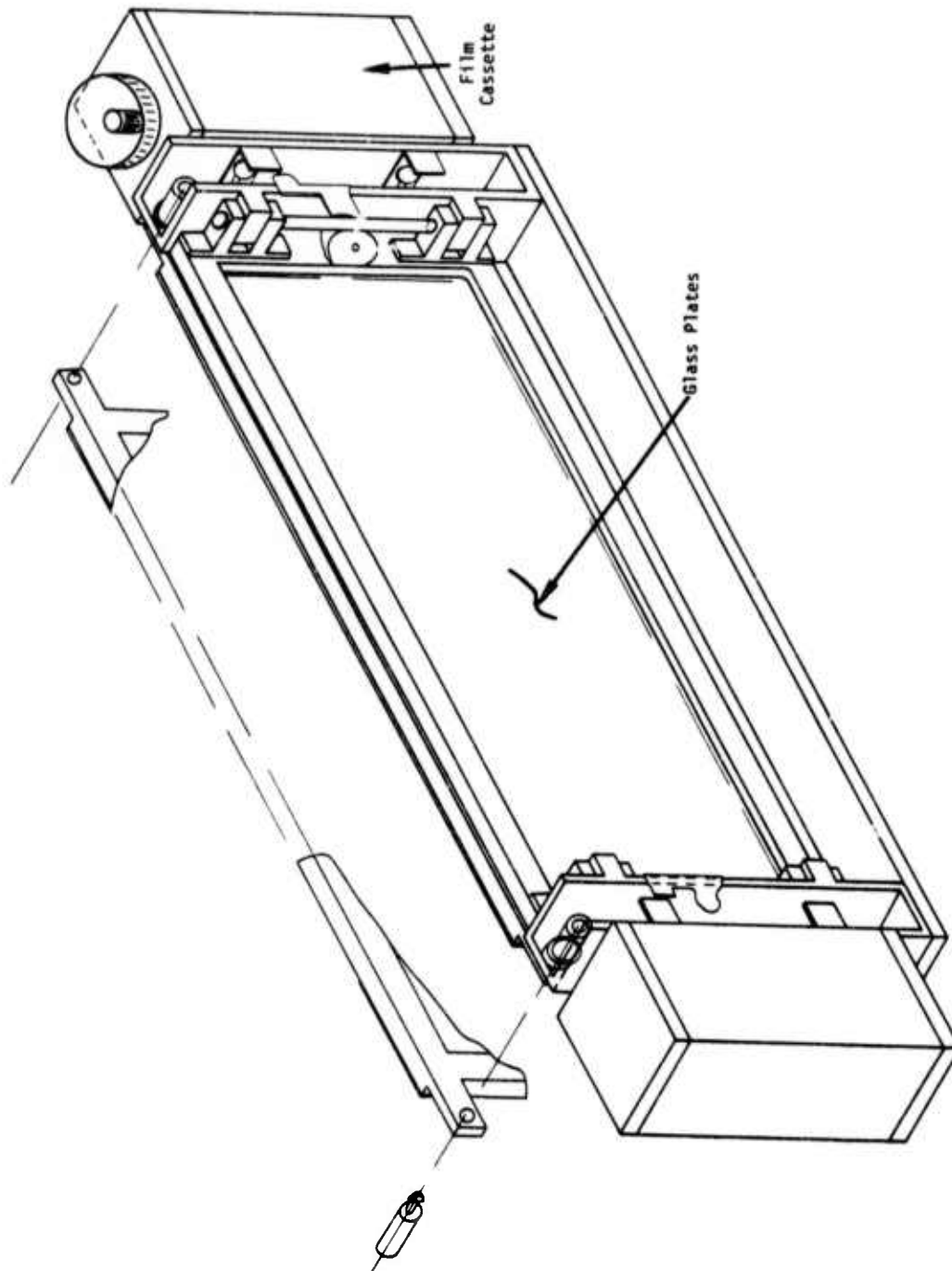
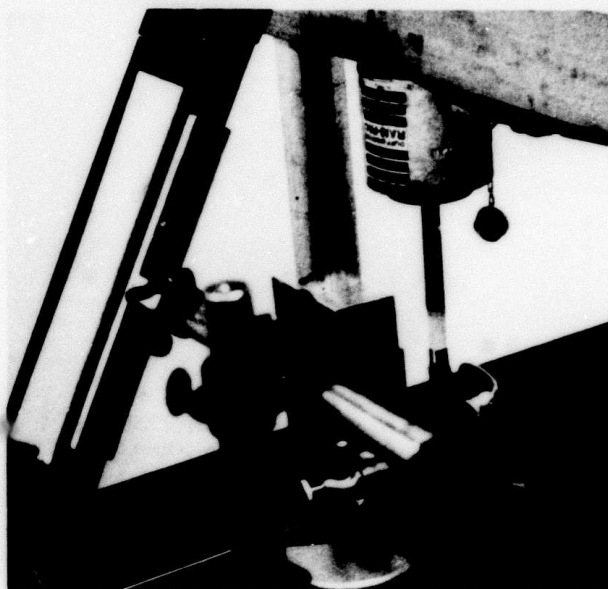Figure 12:   Artist drawing of the holographic interferogram recorder.

Figure 13: The holographic interferogram recorder being used in our axial load test.

4.0 HOLOGRAPHIC UNIAXIAL TESTS ON TWO SOFT ROCKS

Holographic interferometry was used successfully to obtain full field radial and axial displacement data along the axis of cylindrical specimens of Mixed Company Sandstone and Limestone during a uniaxial and triaxial compressive test. The uniaxial tests were carried out with the same setup as the triaxial test except the pressure vessel was removed. A sandstone specimen is shown in Figure 14.

4.1 Test Description

The geometry of the holographic setup used in these tests is shown schematically in Figures 15 and 16. From a top view of the setup (Figure 15) the illumination of the specimen and viewing (camera) was along a common axis. This was necessary due to the constricting aperture of the pressure vessel window. The angles made between the
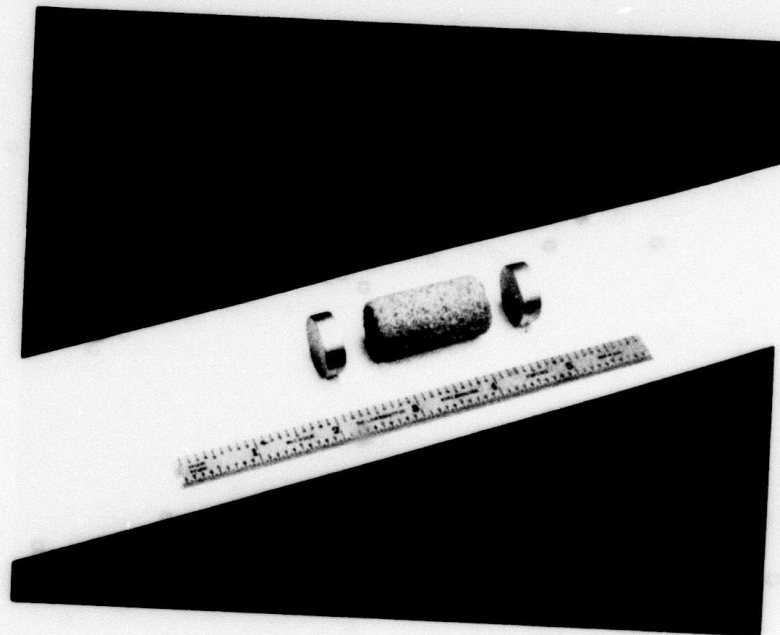
Figure 14: Specimen of Mixed Company Sandstone with end caps. The combination is enclosed in transparent shrinkable tubes during triaxial holographic test.
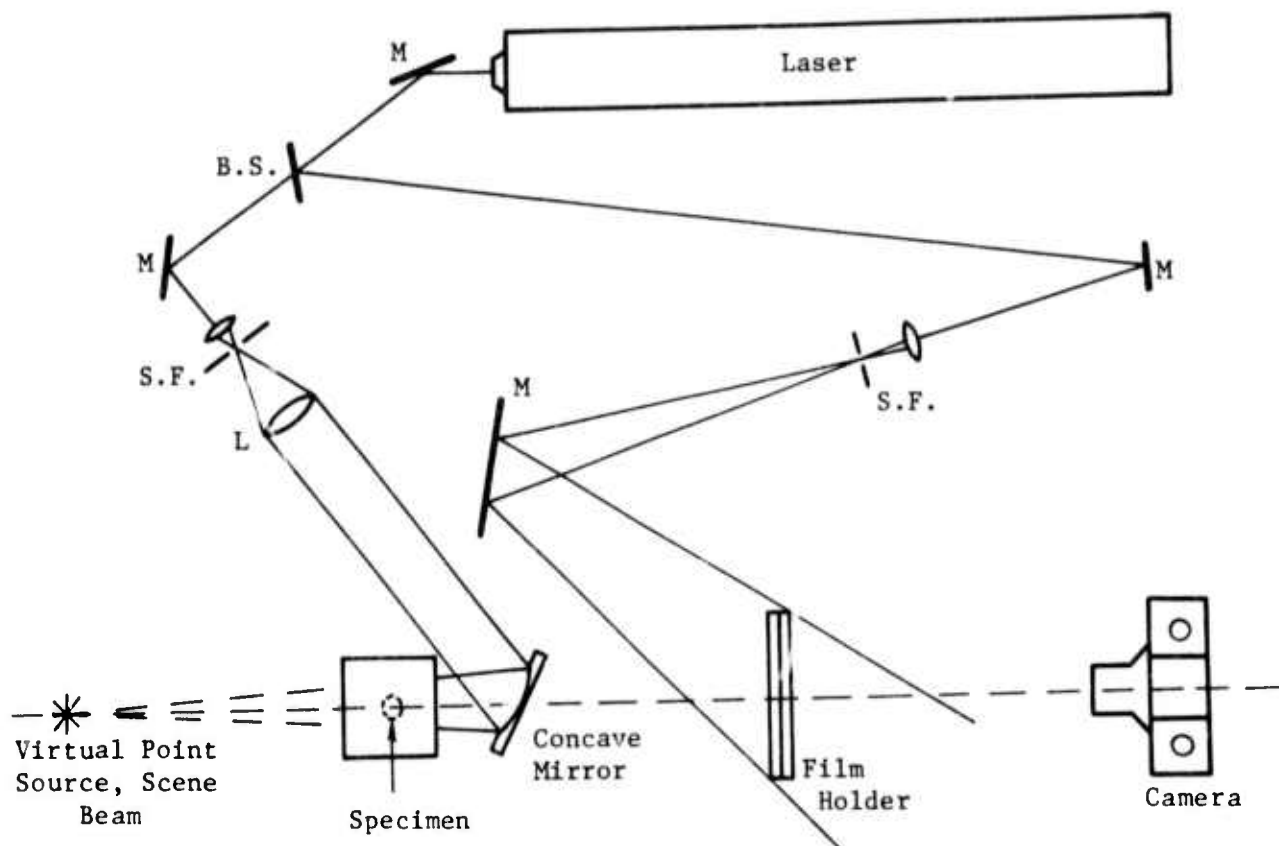
Figure 15: Top view of holographic setup for testing rock specimens under axial and triaxial loads.
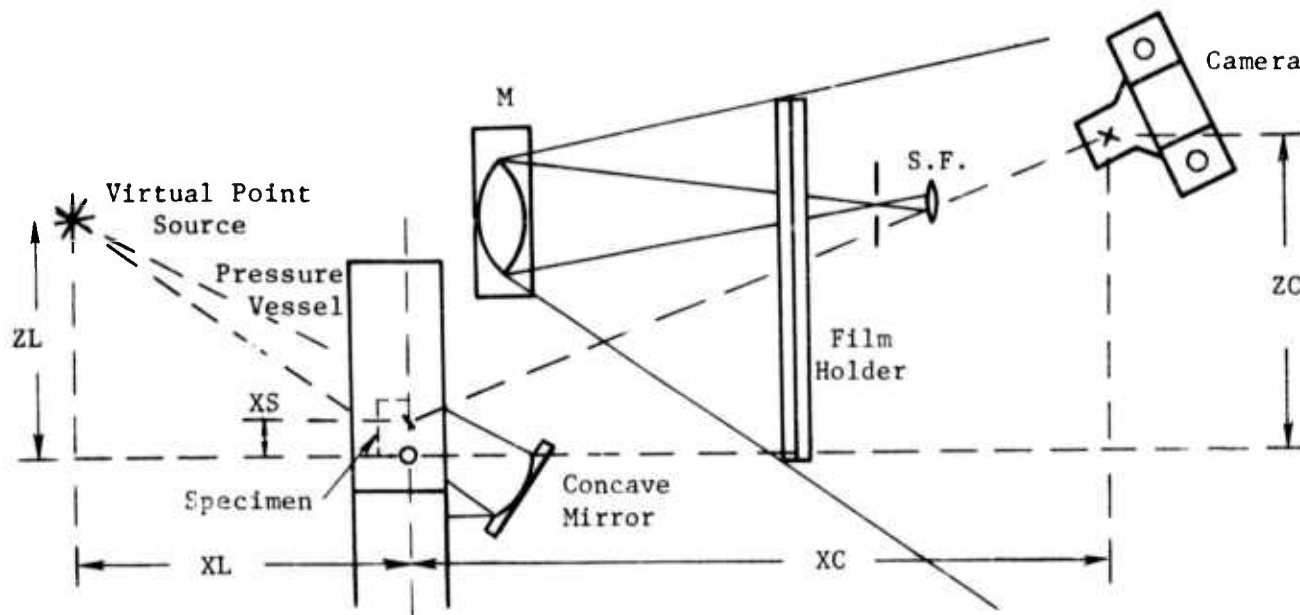
Figure 16: Side view of holographic setup. M – Mirror, S.F. – Spatial Filter, B.S. – Beam Splitter. The geometrical measurements ZL,XL,ZC,XC, & XS are necessary for the data reduction.

TRW
SYSTEMS GROUP

specimen surface and the illumination and viewing paths are shown in the side view (Figure 16). The values XL and ZL for the laser source position and XC and ZC for the camera viewing position were measured and used to calculate the coefficients in Eqs. (9) and (10).

The concave mirror used to focus the scene beam onto the specimen inside the pressure vessel served two purposes. It concentrated the laser light onto the specimen from an expanding beam at the spatial filter. Second, it created a virtual point source for the laser source. This provided a simple geometry for describing to the computer code.

A single spatially filtered diverging beam was used as a reference beam to illuminate the full 15 inch length of the holographic film held in the interferogram recorder. It was found that two overlapping reference beams on the same film caused a lack of continuity in image brightness and contrast at the position of overlap. This made it difficult to keep track of fringes and photograph them.

A typical test procedure was as follows: Once the specimen was in place a small preload was placed on it to insure stability to the loading structure during the first interferogram load increase. A photographic plate or film was then loaded into the holder. A reference exposure of the specimen was made at the reference load (P_r). The load on the specimen was then increased by a predetermined amount (ΔP). This amount is dependent on the number of fringes it will produce. The second exposure was made at the new load $(P_r + \Delta P)$. A new photographic plate or film frame was moved into place and the same procedure repeated. Thus, a single interferogram was recorded for each step load.

To reduce the interferograms to displacement fields required first that photographs be taken of the fringe patterns from several viewing directions through the reconstructed holograms. The holograms were reconstructed in the same setup to preserve magnification and insure the correct description of the holographic geometry. The fringe

27

patterns obtained in each photograph were then digitized. This
digitized fringe information was then used along with the holographic
geometry to calculate the displacement fields over the surface of
the specimen using the developed computer code and the approach given
in the previous section.

In the triaxial tests corrections were made for the refraction
of the ray paths through port windows and the pressurized water.

4.2 Results of Uniaxial Tests on Mixed Company Sandstone

The Mixed Company Sandstone specimens were obtained from Terra Tek
and were labeled as coming from P.I. hole #4. The specimen dimensions
were approximately .70 in. by 1.4 in. in length. The circumferential
surface of the specimen was left untouched for the test. The ends of
the cylindrical specimens were ground as nearly flat and parallel as
possible.

The specimen was preloaded to 1000 psi before the first hologram
was taken to take the play out of the loading structure. Three
interferograms were taken in loading steps of 350 psi each. A
representative photograph of the fringe pattern from each of the three
interferograms (load steps) is shown in Figure 17 A,B,& C.

The fringe positions are plotted along the center of the specimen
for each interferogram in Figure 18 A,B, & C. The four curves in each
figure represents fringe patterns from each of four photographs taken
from four different directions through the holographic film aperture.

The fringe patterns plotted in Figure 18 were then used to calculate
the radial and axial displacements at points along the axis. The
relative fringe orders from one photograph to the next are critical
to determining the magnitude of calculated axial and radial displacements.
The fringe orders were properly labeled by always using one photograph
(taken at the same location) as a reference. The first fringe at the
bottom of the specimen in this reference photo was given a fringe
order of -1. The remainder of the fringes were labeled in negative
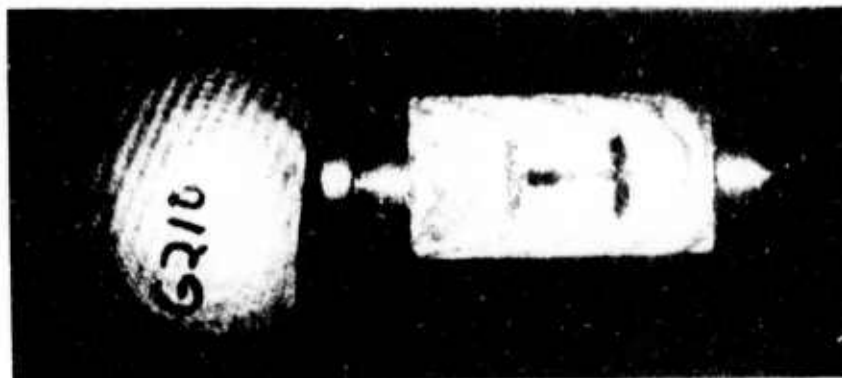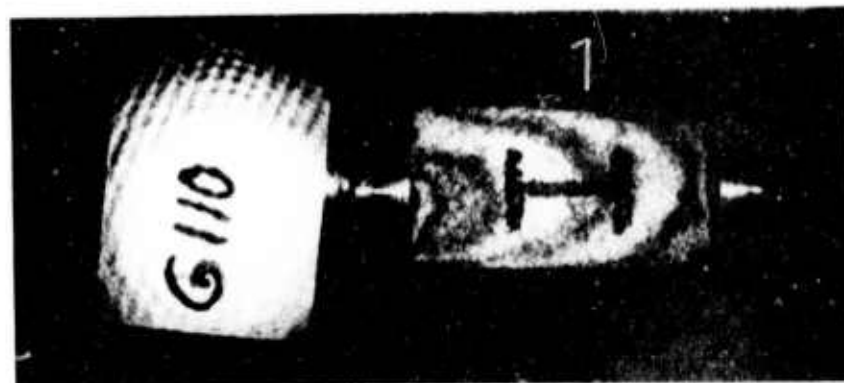
Figure 17: Photographs of Mixed Company Sandstone interferograms taken during uniaxial tests. Photo A represents a load step of 1000 psi to 1350 psi; photo B 1350 to 1700 psi and photo C 1700 to 2050 psi.
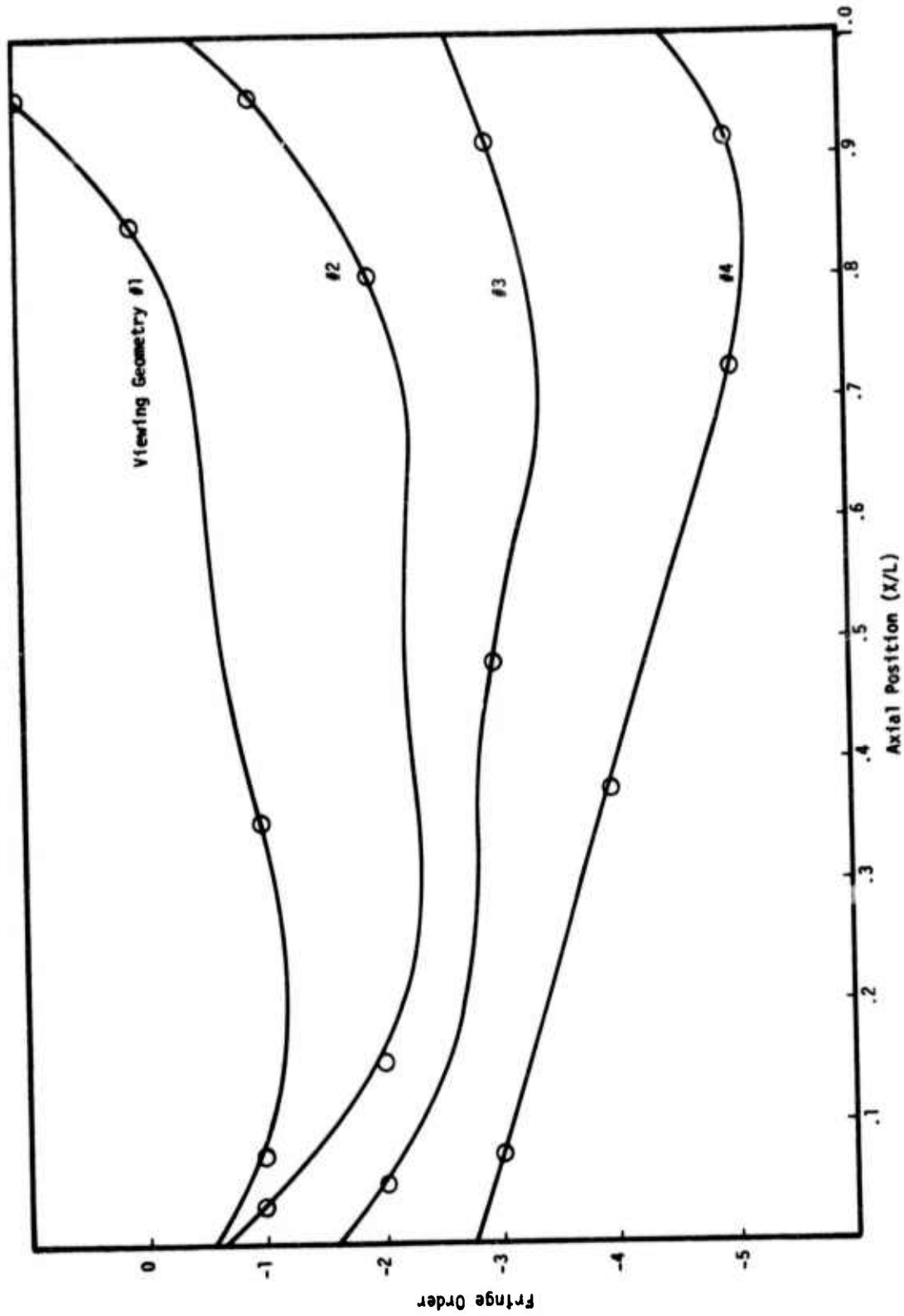
Figure 18A: Fringe fields from four viewing positions for the same interferograms. The stress increment from the interferogram was 1000 psi to 1350 psi.
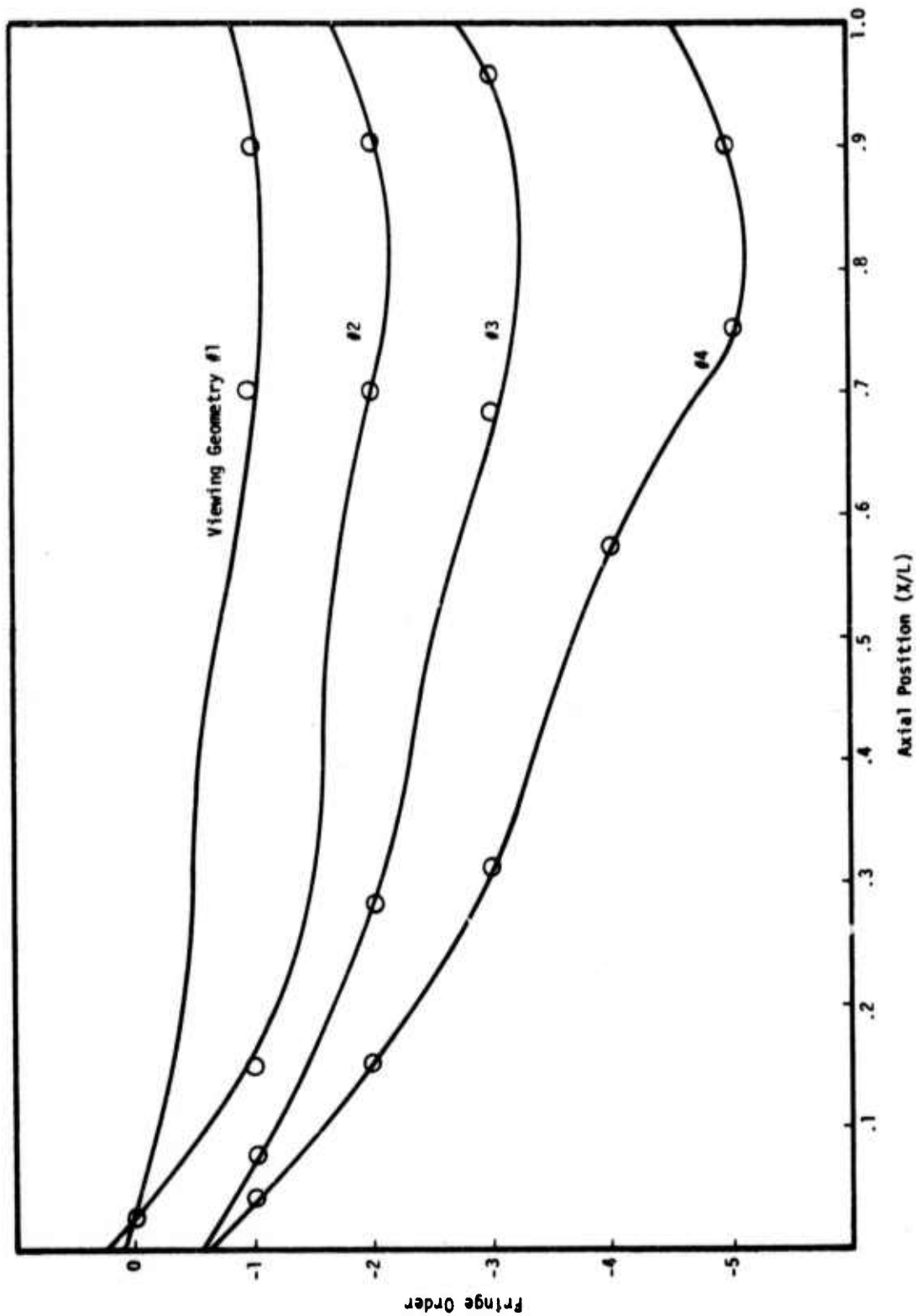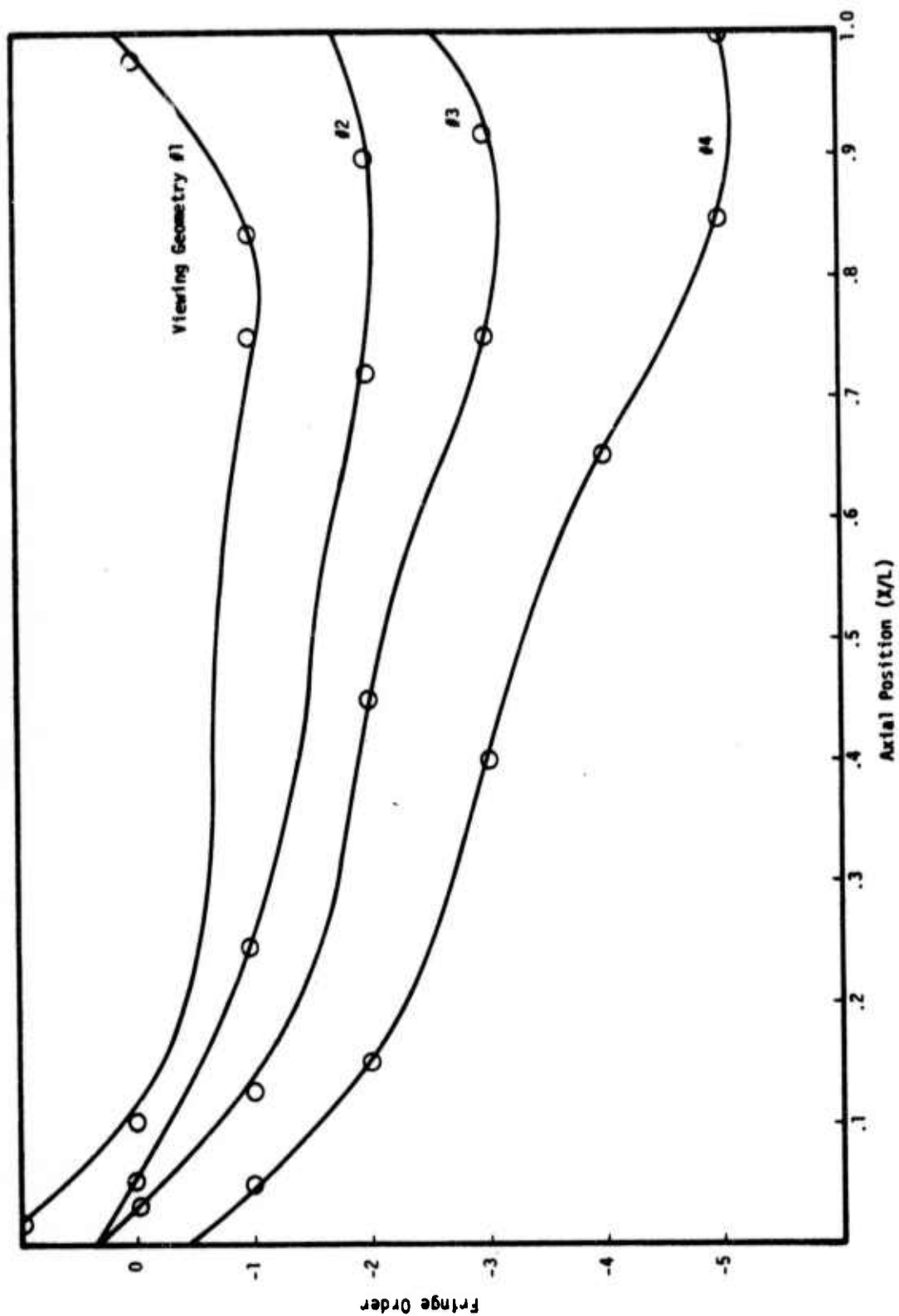
Figure 18B: Fringe fields from four viewing positions for the same interferogram. The stress increment for the interferogram was 1350 psi to 1700 psi.

TRW
SYSTEMS GROUP

Figure 18C: Fringe fields from four viewing positions for the same interferogram. The stress increment for the interferogram was 1700 psi to 2050 psi.

32

TRW
SYSTEMS GROUP

sequence. Fringe orders in subsequent photos are simply determined by observing the fringe shift across the end boundary of the specimen from one hologram viewing position to the next.

The radial displacements for each load step as calculated from the fringe patterns are displayed in Figure 19 A,B, & C. Figure 19D gives the total radial displacements from the three interferograms.

It was necessary to correct the recorded radial displacement values for rigid body tilt of the specimen during loading. To accomplish this it was assumed that the ends of the specimen did not expand during the test. The curves were corrected for tilt by taking the difference between the absolute data and a straight line drawn between the extrapolated end points of the data. Corrections for tilt in this manner yielded the radial displacement profiles shown in Figure 20 A,B,C & D. The tilt amounted to approximately 5 μrad. This is equivalent to a displacement of $.5 \times 10^{-3}$ inches over a 15 inch lever arm. This amount of tilt is understandable for the load structure used.

The large uncertainty in the magnitude of the radial displacement profile along the specimen is a result of axis uncertainty in the magnitude of the radial expansion at the ends of the specimen and the necessity of extrapolating the data at the end points. However, the shape of the radial displacement profiles is believed to be accurate. This uncertainty in the baseline of the radial displacement profile can be removed from test results by studying the boundary conditions and/or direct measurement of the rigid body tilt of the specimen during the test. Such rigid body reference measurements could be made with a single lever arm strain gauge at the end cap or with a single linear interferometer measurement off a mirror positioned in the end cap.

Axial displacement profiles for each of the three load steps are plotted in Figure 21 A,B, & C. The total axial displacement profile is plotted in Figure 21D along with the total axial strain distribution profile. The average strain for each of the load steps is compared
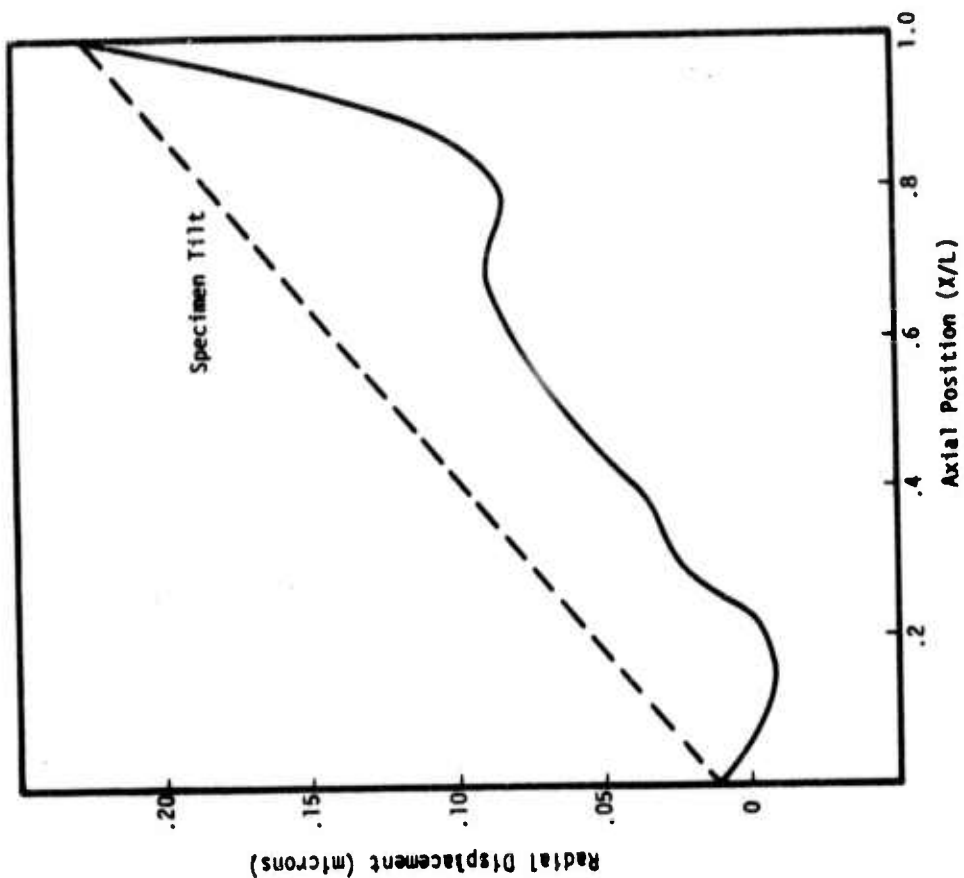
33

Figure 19A: Radial displacement profile along axis of Mixed Company Sandstone specimen. The load increment for this interferogram was 1000 psi to 1350 psi.
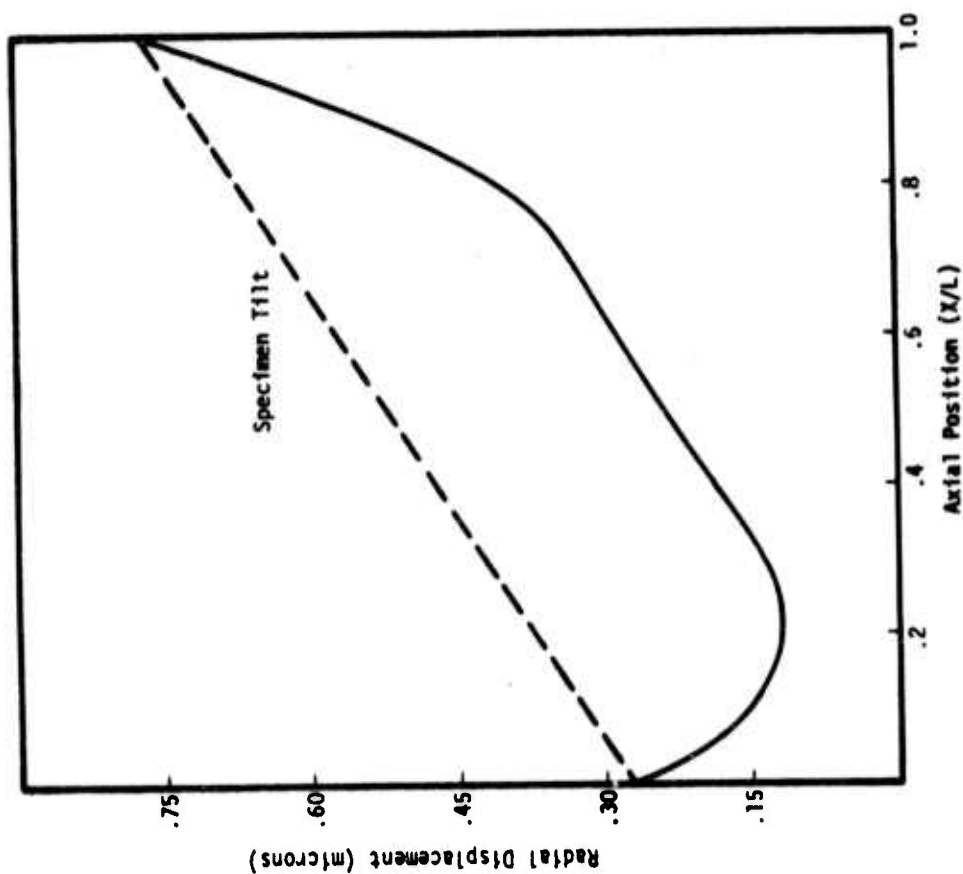
Figure 19B: Radial displacement profile along axis of Mixed Company Sandstone specimen. The load increment for this interferogram was 1350 psi to 1700 psi.
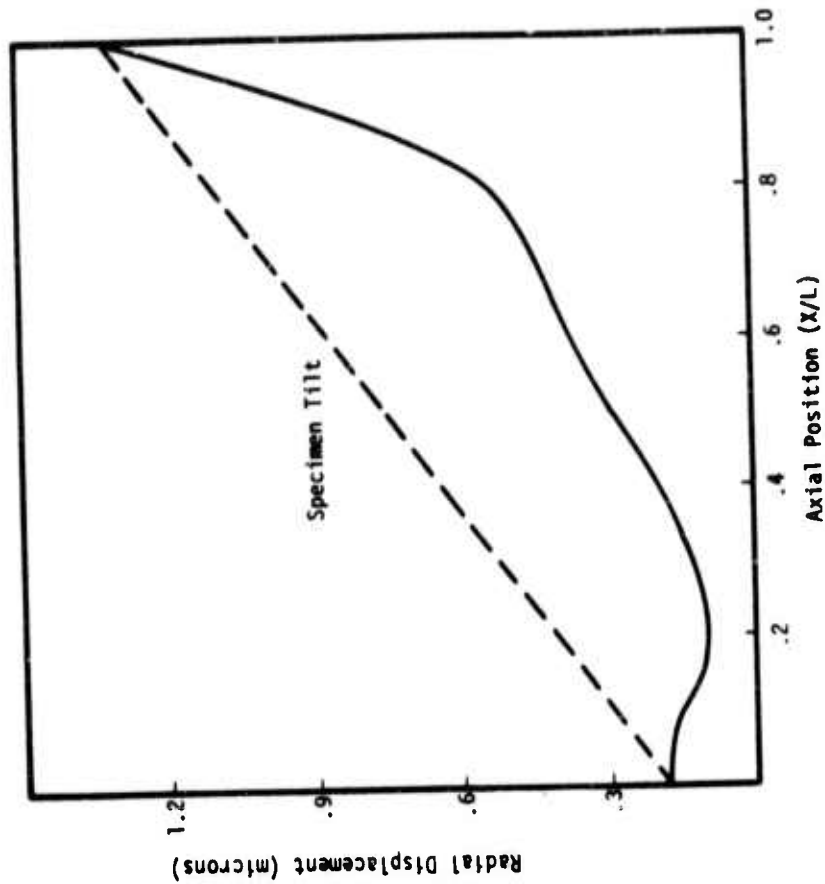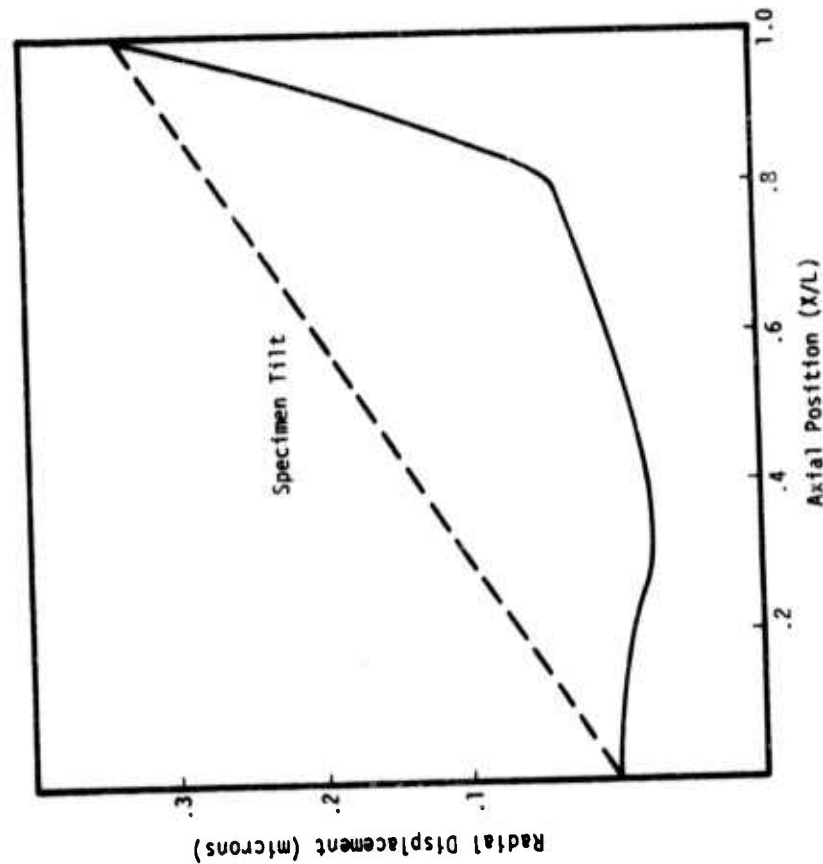
Figure 19D: Total radial displacement profile along the axis of Mixed Company Sandstone specimen for the three interferograms. The total load increase was 1000 psi to 2050 psi.

Figure 19C: Radial displacement profile along axis of Mixed Company Sandstone specimen. The load increment for the interferogram was 1700 psi to 2050 psi.

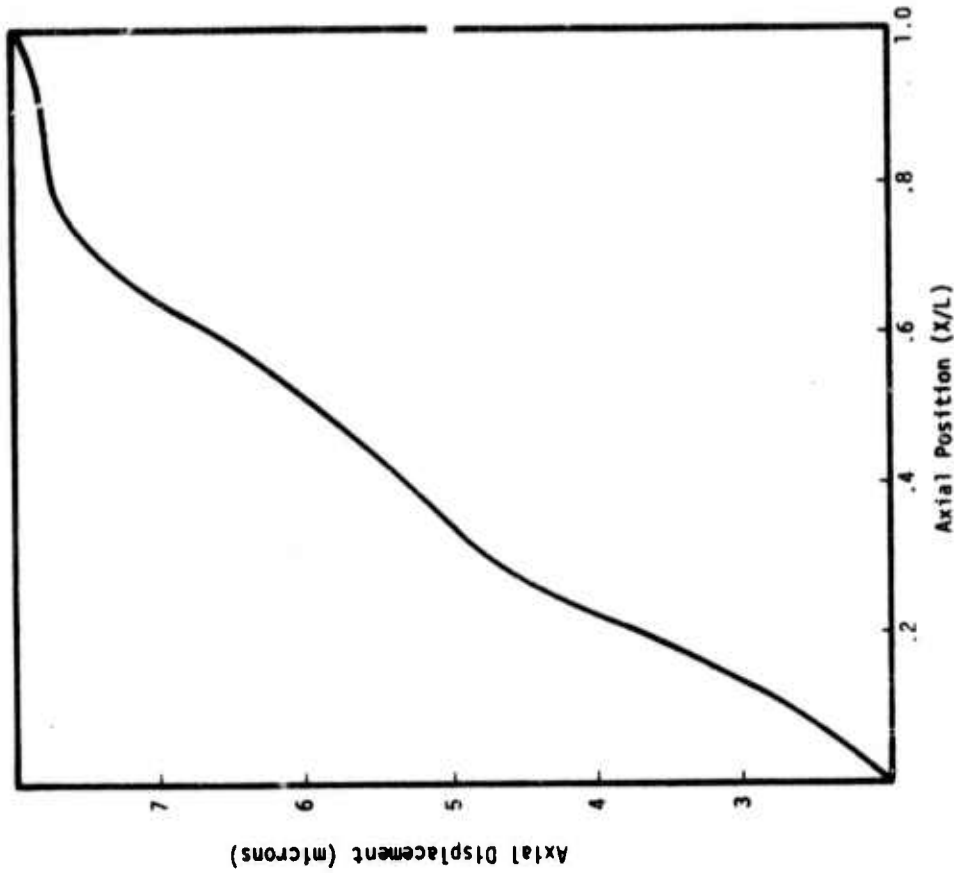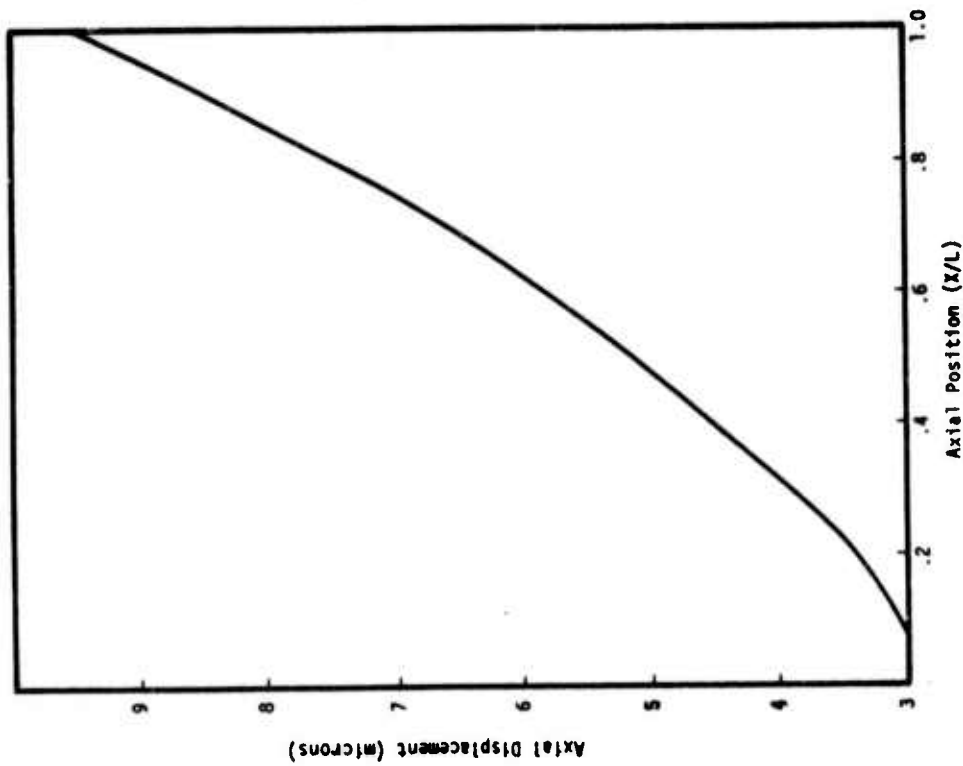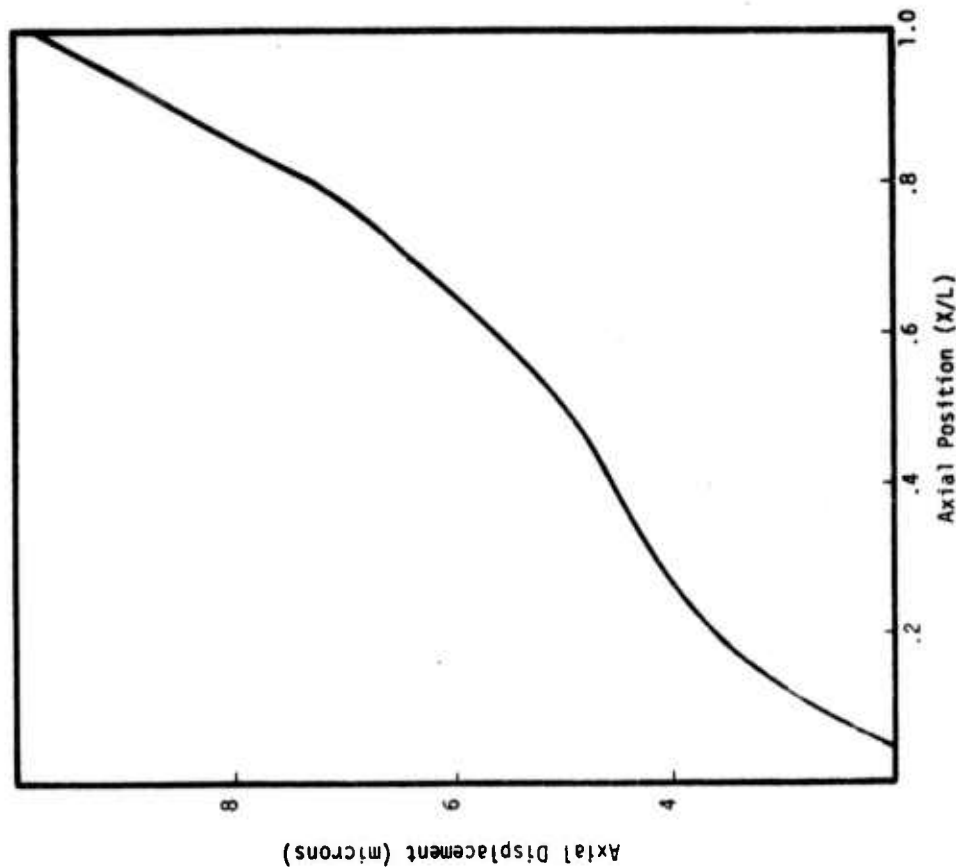Figure 20B: Radial displacement profile corrected for specimen tilt. Load increment 1350 psi to 1700 psi.
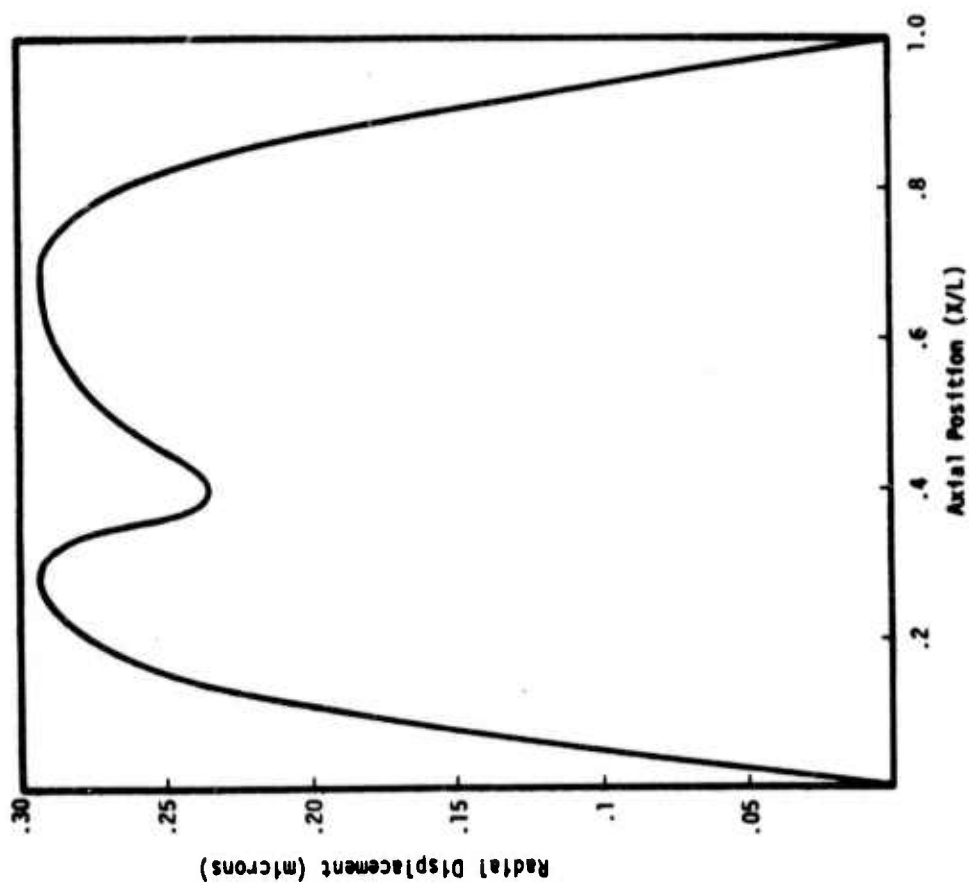
Figure 20A: Radial displacement profile corrected for specimen tilt. Load increment 1000 psi to 1350 psi.
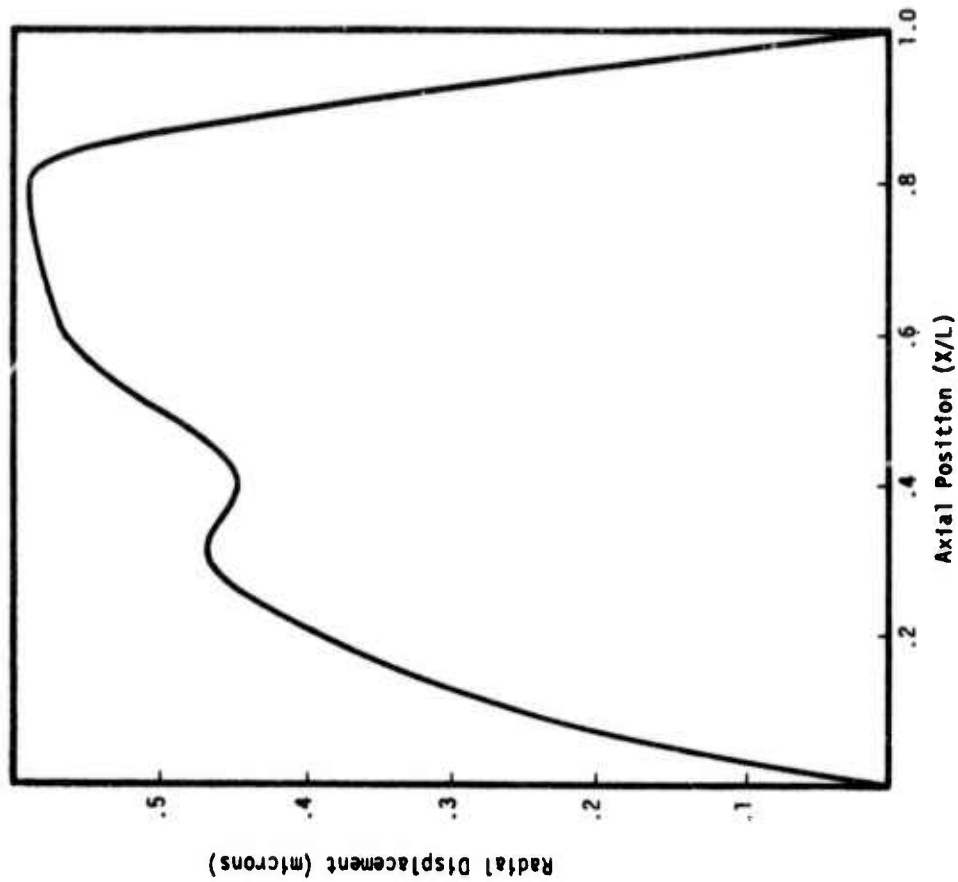
Figure 20D: Total radial displacement profile for uniaxial test on Mixed Company Sandstone. Load increment 1000 psi to 2050 psi.
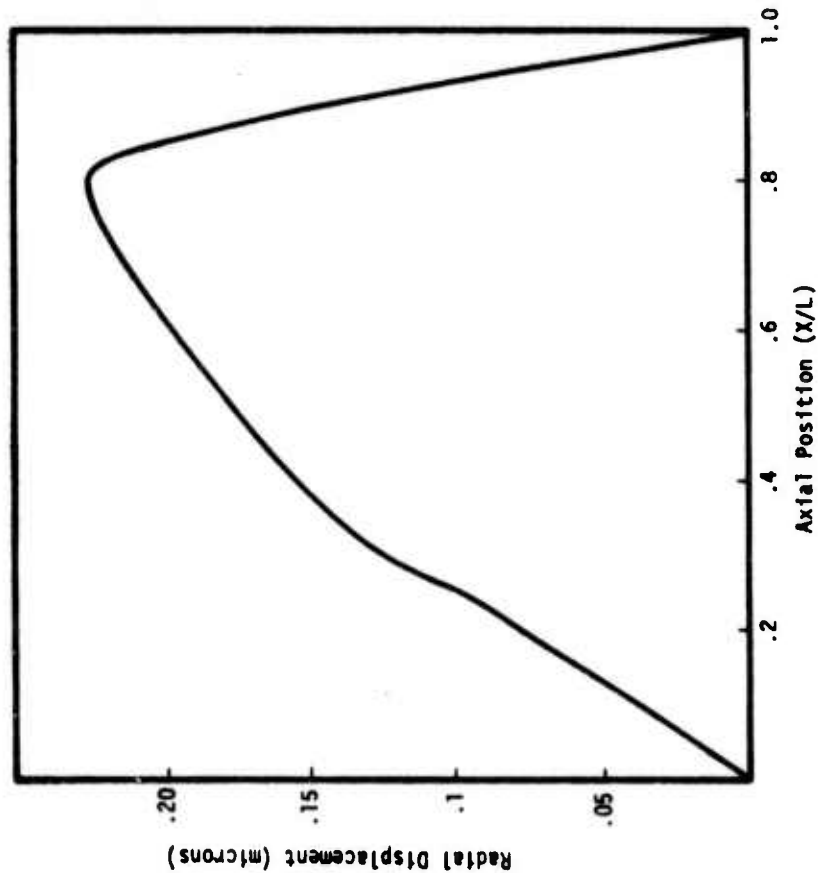
Figure 20C: Radial displacement profile corrected for specimen tilt. Load increment 1700 psi to 2050 psi.

Figure 21A: Axial displacement profile along axis
of Mixed Company Sandstone specimen.
Load increment 1000 psi to 1350 psi.

Figure 21B: Axial displacement profile along axis
of Mixed Company Sandstone specimen.
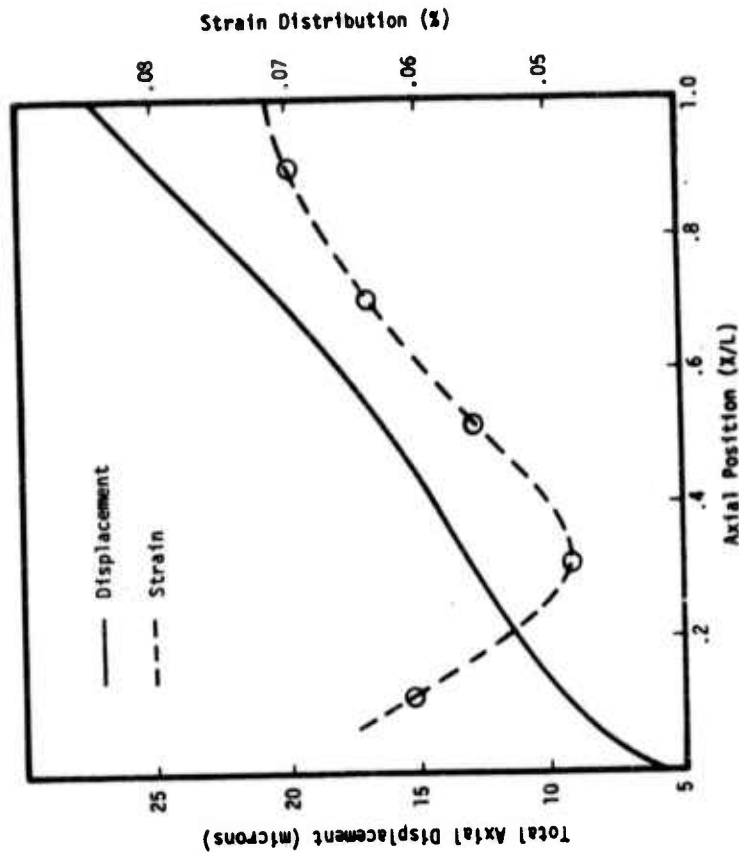Load increment 1350 psi to 1700 psi.

Figure 21D: Total axial displacement profile and strain distribution along axis of Mixed Company Sandstone specimen. Total load increment 1000 psi to 250 psi.

Figure 21C: Axial displacement profile along axis of Mixed Company Sandstone specimen. Load increment 1700 psi to 2050 psi.

39

with uniaxial data obtained in the conventional manner by Terra Tek
in Figure 22 (private communication). For lack of a reference point,
the preload starting point of 1000 psi was plotted on top of the Terra
Tek data. Although there may be an offset in the data due to the
uncertainty in the total strain at the starting point, the slopes are
in good agreement.

4.3 Results of Uniaxial Tests on Limestone

Holographic interferometry was also used to measure the radial
and axial displacement profiles of cylindrical specimens of limestone
subjected to uniaxial compressive loads. The type of limestone tested
was Lithographic Limestone from Bavaria obtained from Wards Scientific.
The cylindrical specimens were cut to 1.5 inch length by .75 inch
diameter. The ends were ground parallel and placed between end caps
as before.

The test procedure for measurements of the radial and axial
displacement profiles using holographic interferometry was the same
as that for the sandstone specimen. Total radial displacement
measurements along the axis of the specimen were corrected for specimen
tilt during the test by again assuming that the motion of the ends of
the specimen in the radial direction constituted rigid body tilt.

The preload stress for the test was 1000 psi. Stress increments
of 1000 psi were used for each of the interferogram recordings. The
total test range was 1000 psi to 5000 psi for a total of four
interferograms.

A representative photograph used for digitizing the fringe
patterns for data reduction from each of the interferograms is shown
in Figure 23. The fine grain surface of the limestone specimen made
it relatively easy to perform the holographic interferometry.

Radial displacement profiles which have been corrected for specimen
tilt are shown for each of the load increments (interferograms) in

with uniaxial data obtained in the conventional manner by Terra Tek
in Figure 22 (private communication). For lack of a reference point,
the preload starting point of 1000 psi was plotted on top of the Terra
Tek data. Although there may be an offset in the data due to the
uncertainty in the total strain at the starting point, the slopes are
in good agreement.

4.3 Results of Uniaxial Tests on Limestone

Holographic interferometry was also used to measure the radial
and axial displacement profiles of cylindrical specimens of limestone
subjected to uniaxial compressive loads. The type of limestone tested
was Lithographic Limestone from Bavaria obtained from Wards Scientific.
The cylindrical specimens were cut to 1.5 inch length by .75 inch
diameter. The ends were ground parallel and placed between end caps
as before.

The test procedure for measurements of the radial and axial
displacement profiles using holographic interferometry was the same
as that for the sandstone specimen. Total radial displacement
measurements along the axis of the specimen were corrected for specimen
tilt during the test by again assuming that the motion of the ends of
the specimen in the radial direction constituted rigid body tilt.

The preload stress for the test was 1000 psi. Stress increments
of 1000 psi were used for each of the interferogram recordings. The
total test range was 1000 psi to 5000 psi for a total of four
interferograms.

A representative photograph used for digitizing the fringe
patterns for data reduction from each of the interferograms is shown
in Figure 23. The fine grain surface of the limestone specimen made
it relatively easy to perform the holographic interferometry.

Radial displacement profiles which have been corrected for specimen
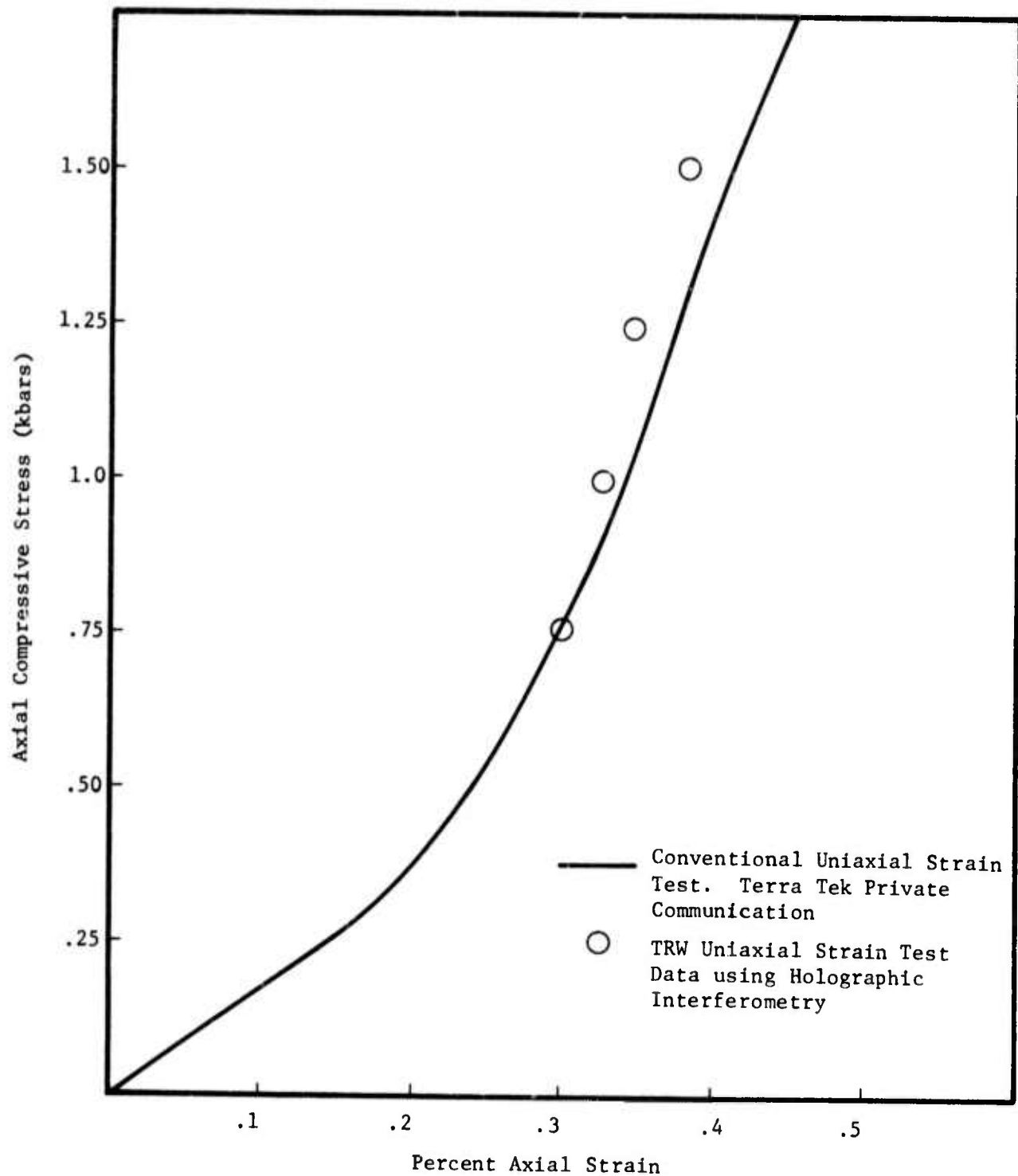tilt are shown for each of the load increments (interferograms) in

Figure 22: Comparison of test data for Mixed Company Sandstone for holographic interferometry and conventional strain gauge measurement techniques.
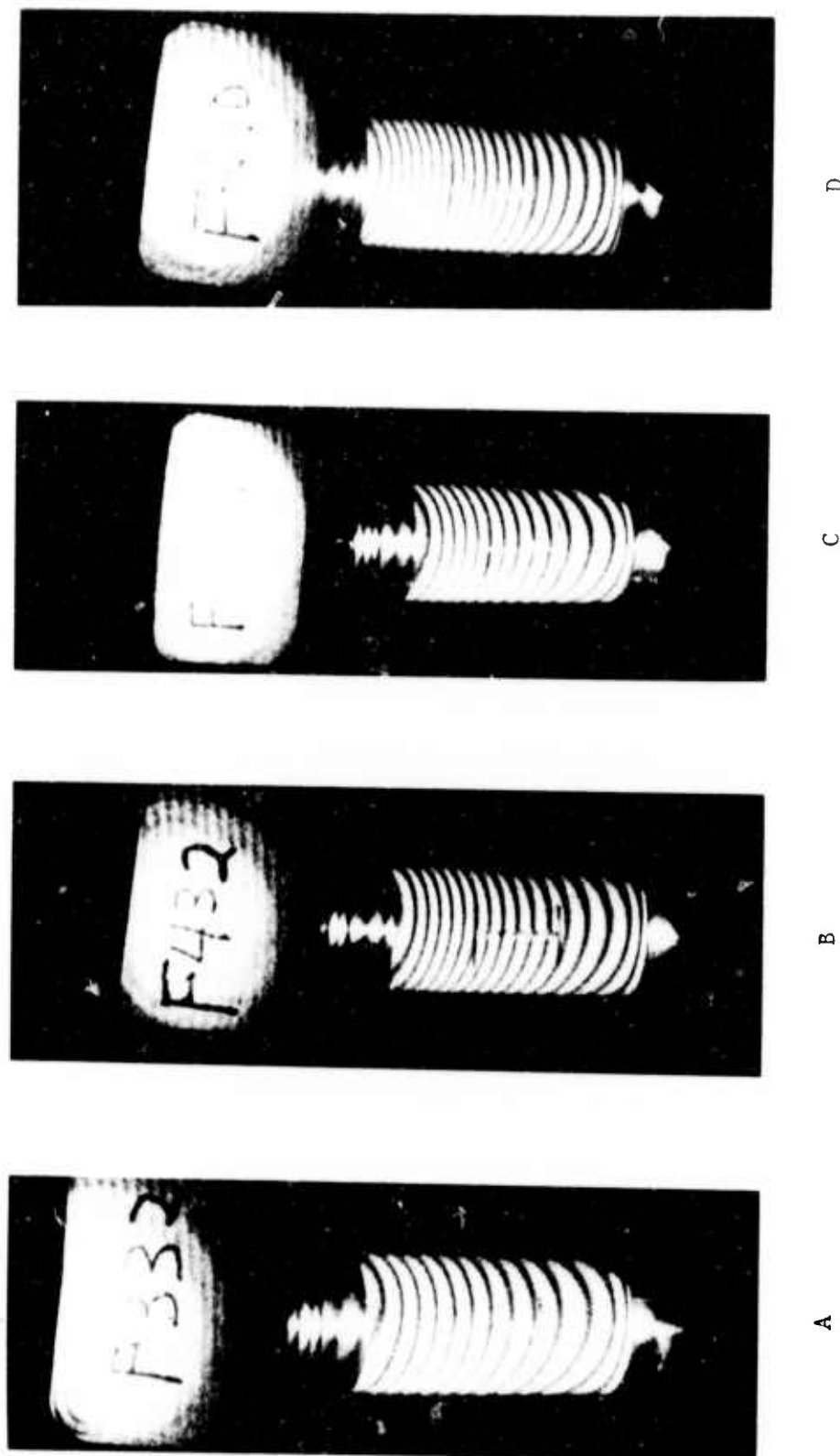
Figure 23: Holographic interferograms of a limestone specimen stressed in uniaxial compression. Each interferogram represents an individual load step during the test. A = 1000 psi to 2000 psi; B = 2000 psi to 3000 psi; C = 3000 psi to 4000 psi; D = 4000 psi to 5000 psi.

Figure 24 A,B,C & D. Axial displacement profiles from each interferogram are shown in Figure 25 A,B,C & D. The sum of the radial displacement profiles (the sum of the four load steps) and the total axial displacements for the test are given in Figure 26 A & B. Figure 26B also shows the axial strain distribution over the length of the specimen. Finally, the total axial strain and total peak radial strain are plotted for the four interferograms in Figure 27 A & B. From the axial and radial strain data, Poisson's ratio is computed to be .22 using the peak radial displacement from the measured profiles.

4.4 Results of Triaxial Tests on Mixed Company Sandstone

The sandstone specimen was prepared for the triaxial test by encapsulating it in a polyurethane shrink tubing and two steel end caps as shown in Figure 6. Water was used for the hydrostatic pressurizing fluid for this test. However, there is no reason why a transparent oil cannot be used which has a known index of refraction.

The hydrostatic pressure σ_3 for the test was held at 4000 psi $\pm$ 50 psi. Two successful holograms were obtained for load steps, $[\Delta(\sigma_1 - \sigma_3)]$, of approximately 250 psi and 400 psi respectively. The total axial load cycle $(\sigma_1 - \sigma_3)$ was from approximately 1000 psi to 1650 psi. There was a large uncertainty in these load measurements due to the necessity of using a low accuracy pressure gauge after the pressure vessel load cell failed from water seepage.

A photograph from each of the two triaxial test interferograms is shown in Figure 28 A & B. Part of the specimen is shadowed due to the photos being taken at an off axis angle through the pressure vessel rectangular viewing port.

The commercial sight glass used as a port window did present some problems in performing the holography. Although the 1/2 inch thick window was strong enough to withstand 5000 psi of pressure, its optical quality was poor. However, high strength optical quality glass can be made from synthetic sapphires (Ref. 1). Much higher pressures
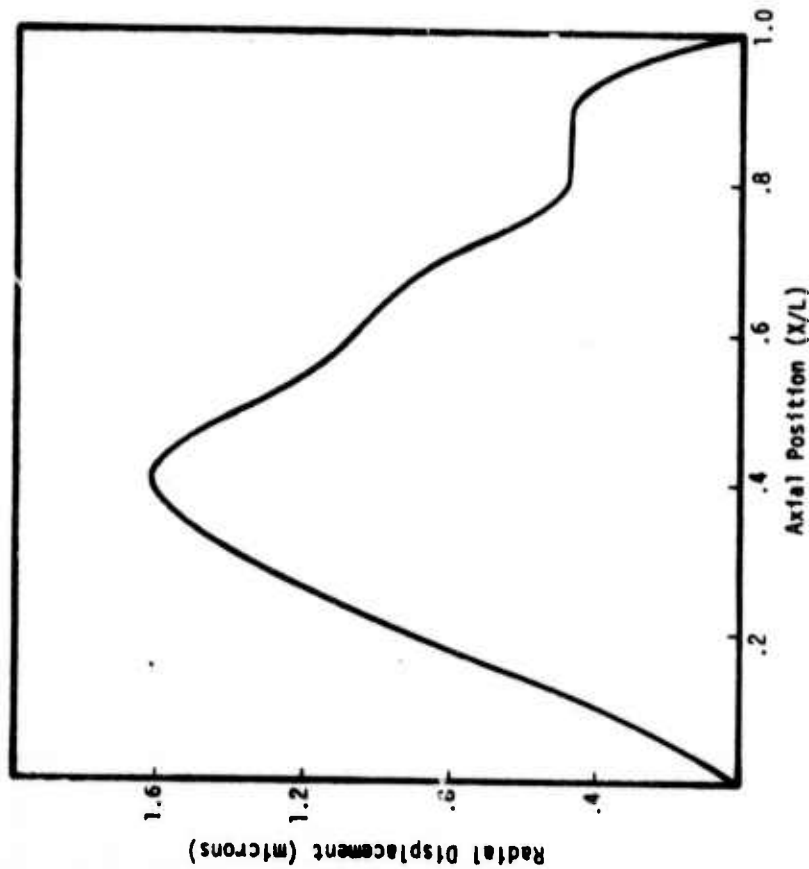
Figure 24A: Radial displacement profile along axis of uniaxial stressed Lithographic Limestone specimen. Load increment 1000 psi to 2000 psi.
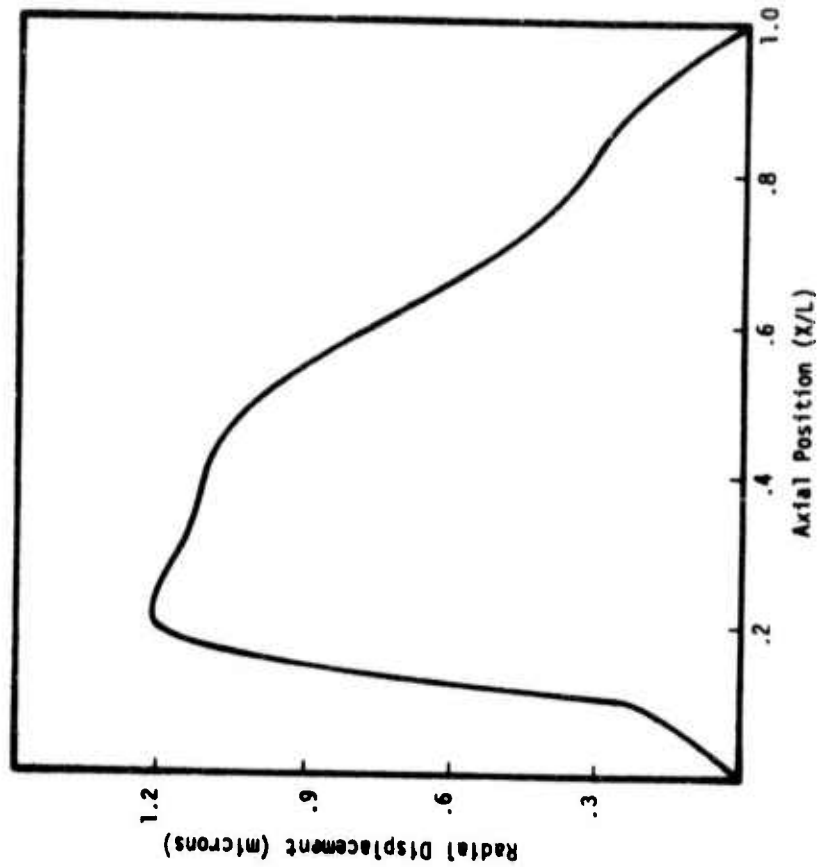
Figure 24B: Radial displacement profile along axis of uniaxial stressed Lithographic Limestone specimen. Load increment 2000 psi to 3000 psi.
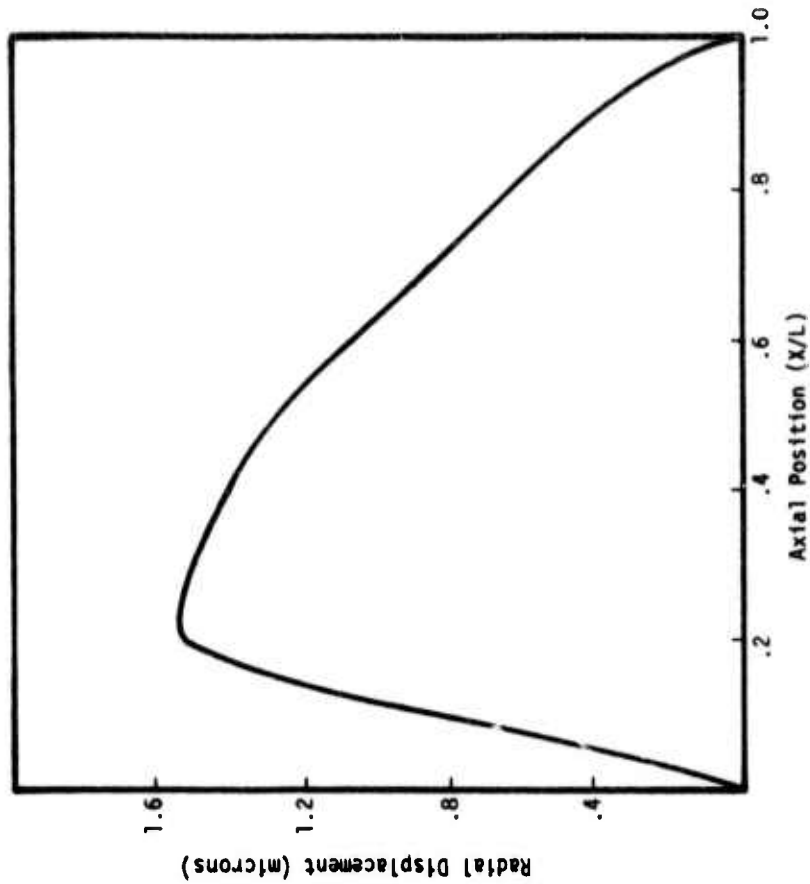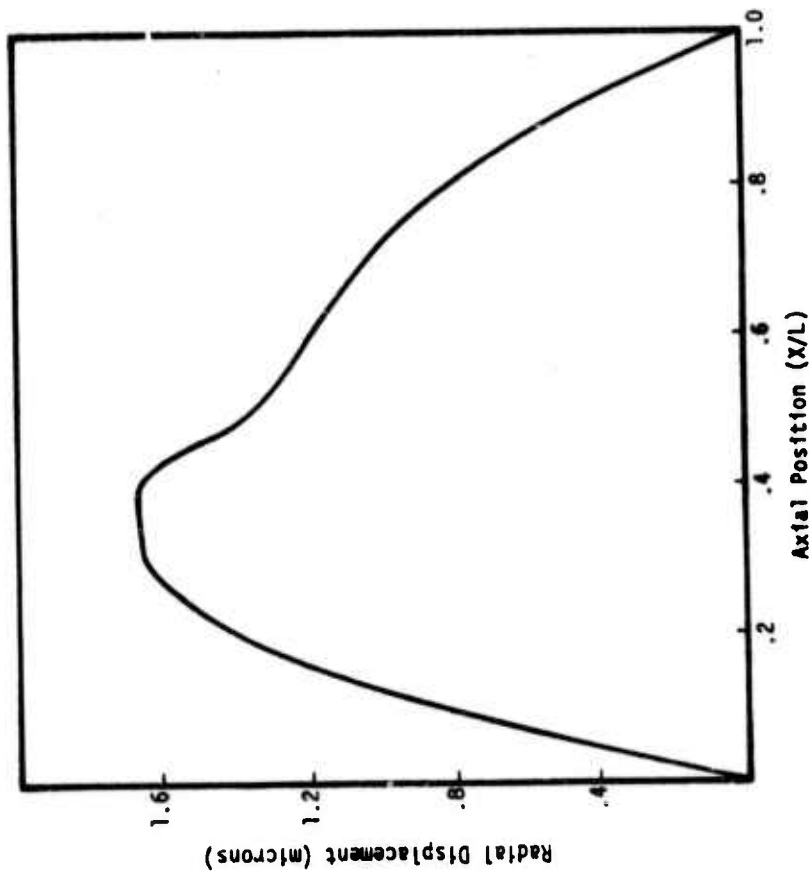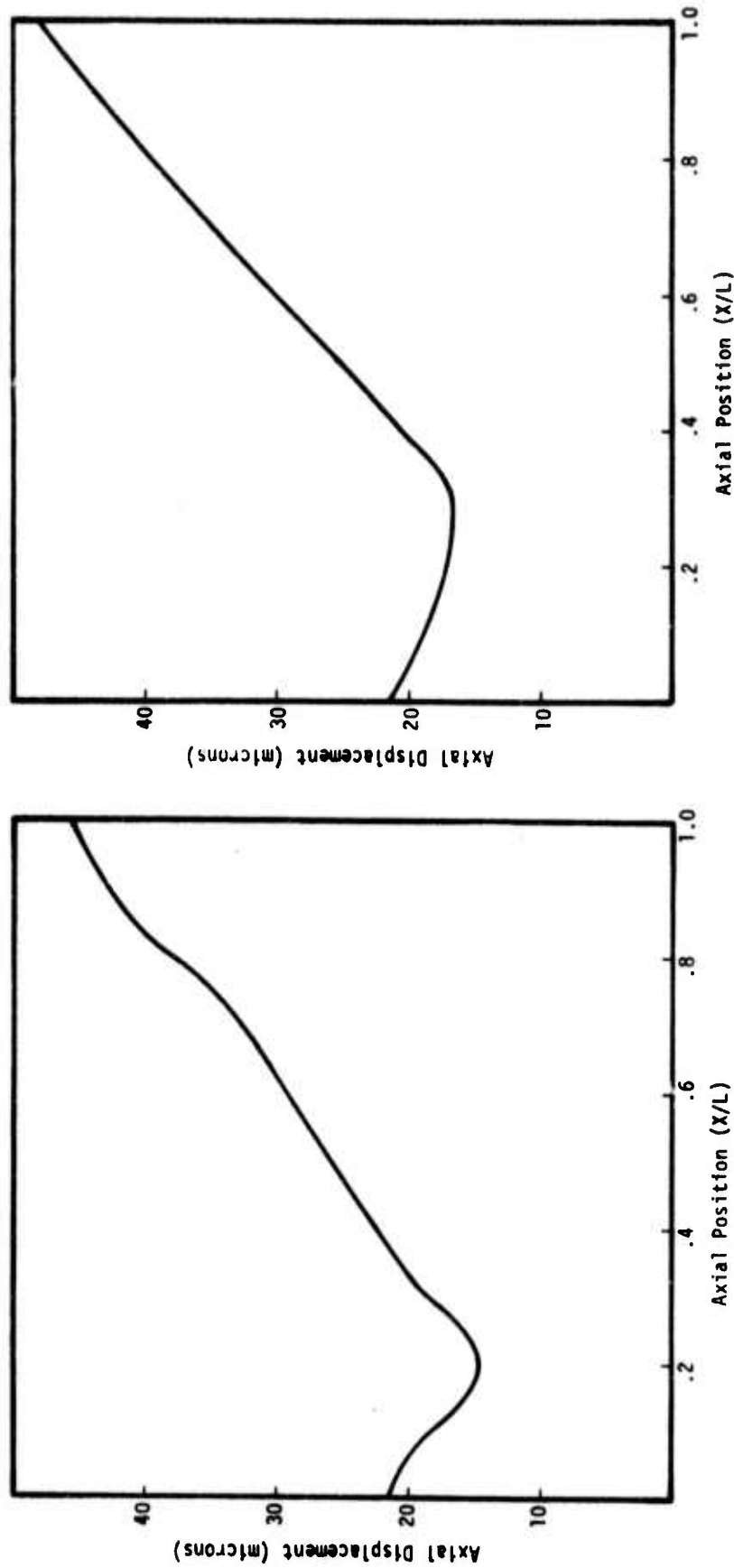
Figure 24D: Radial displacement profile along axis
of uniaxial stressed Lithographic
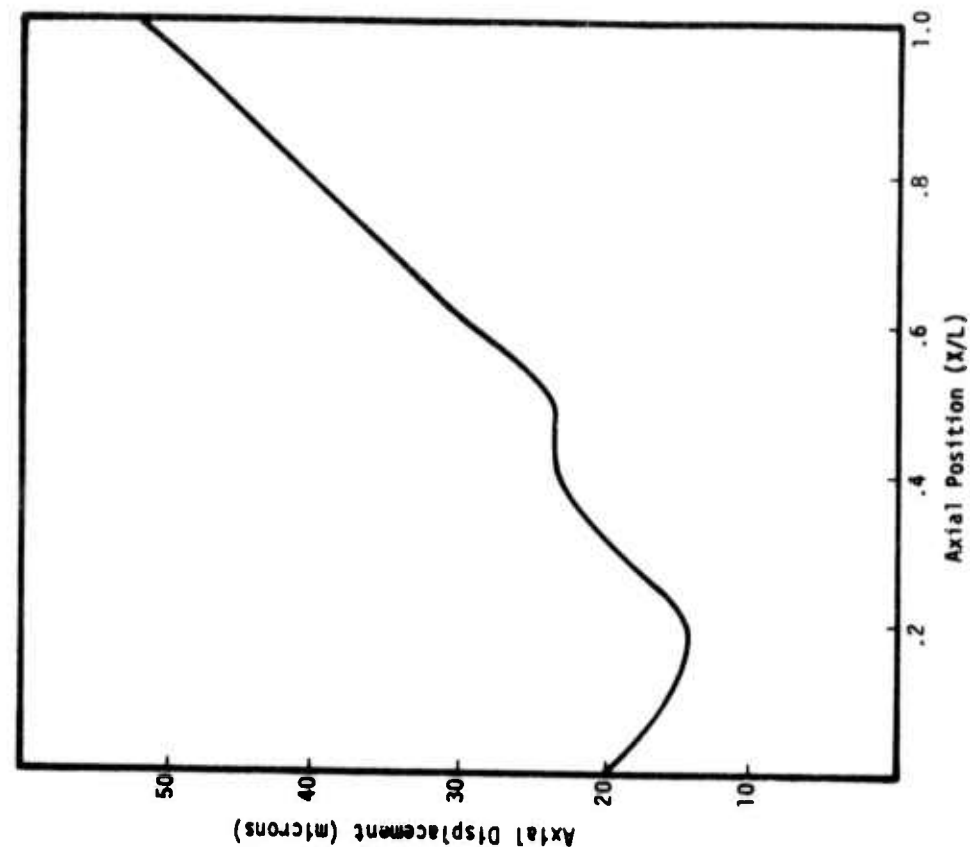Limestone specimen. Load increment
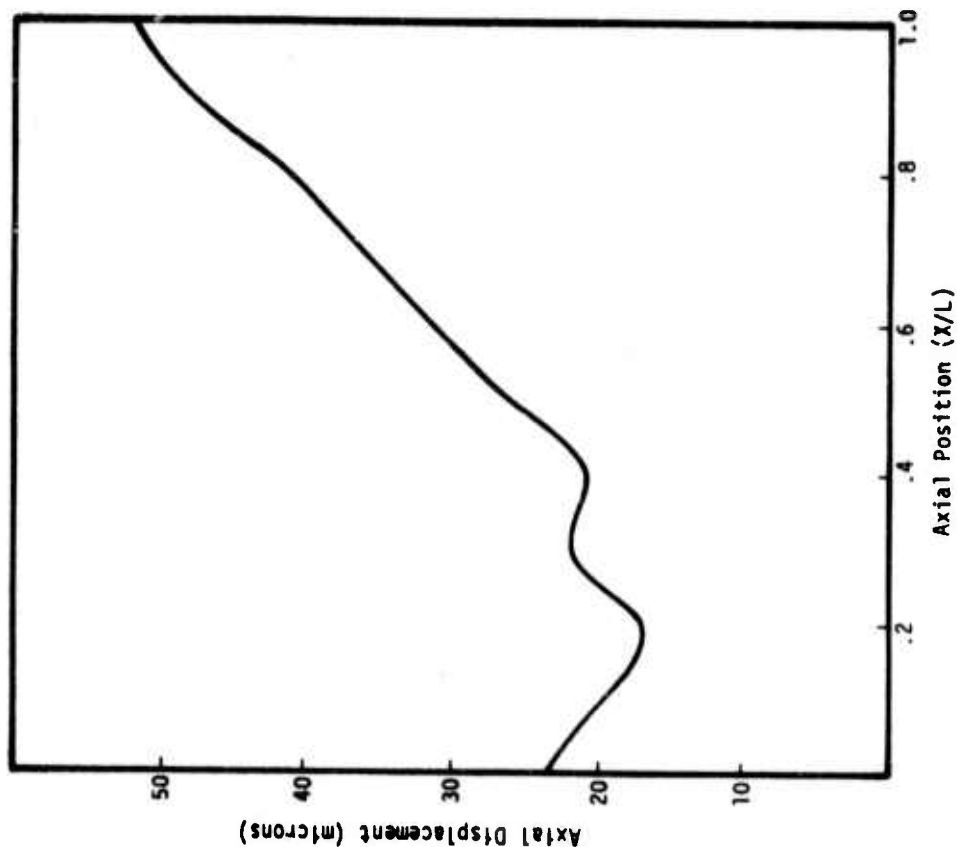4000 psi to 5000 psi.

Figure 24C: Radial displacement profile along axis
of uniaxial stressed Lithographic
Limestone specimen. Load increment
3000 psi to 4000 psi.

Figure 25A: Axial displacement profile along axis of uniaxial stressed Lithographic Limestone specimen. Load increment 1000 psi to 2000 psi.

Figure 25B: Axial displacement profile along axis of uniaxial stressed Lithographic Limestone specimen. Load increment 2000 psi to 3000 psi.
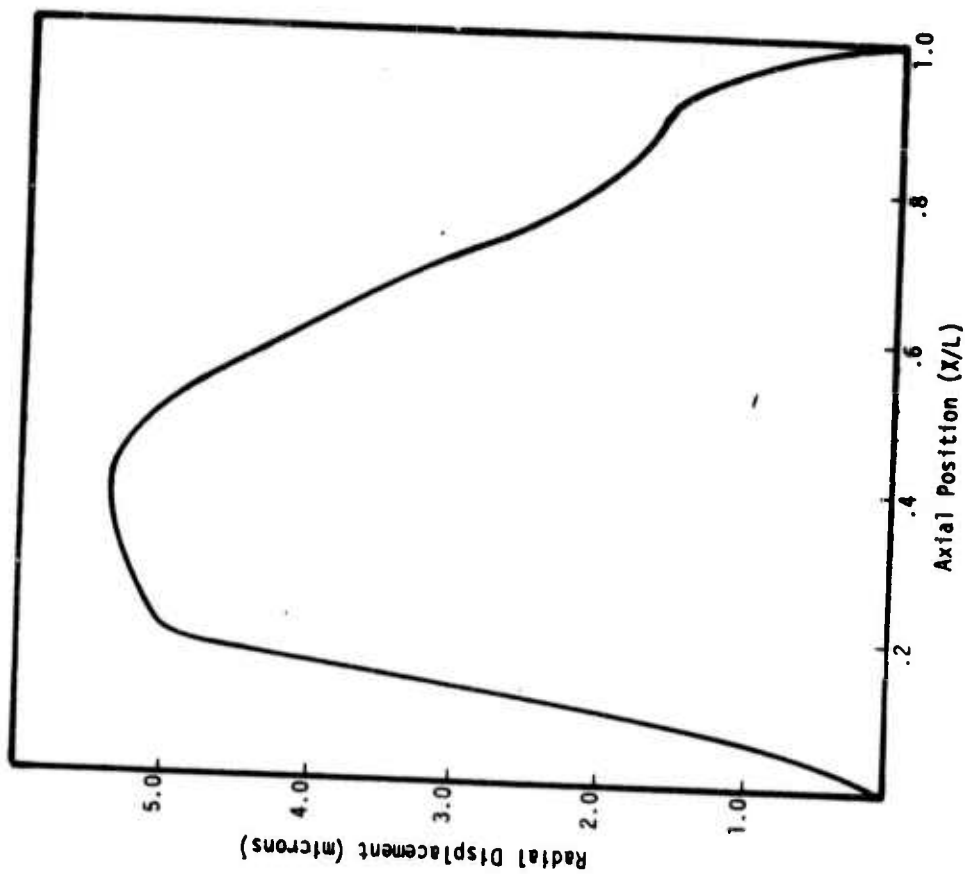
46

TRW SYSTEMS GROUP

Figure 25D: Axial displacement profile along axis of uniaxial stressed Lithographic Limestone specimen. Load increment 4000 psi to 5000 psi.

Figure 25C: Axial displacement profile along axis of uniaxial stressed Lithographic Limestone specimen. Load increment 3000 psi to 4000 psi.

Figure 26A: Total radial displacement profile along axis for uniaxial test on Lithographic Limestone specimen. Total load increment 1000 psi to 5000 psi.
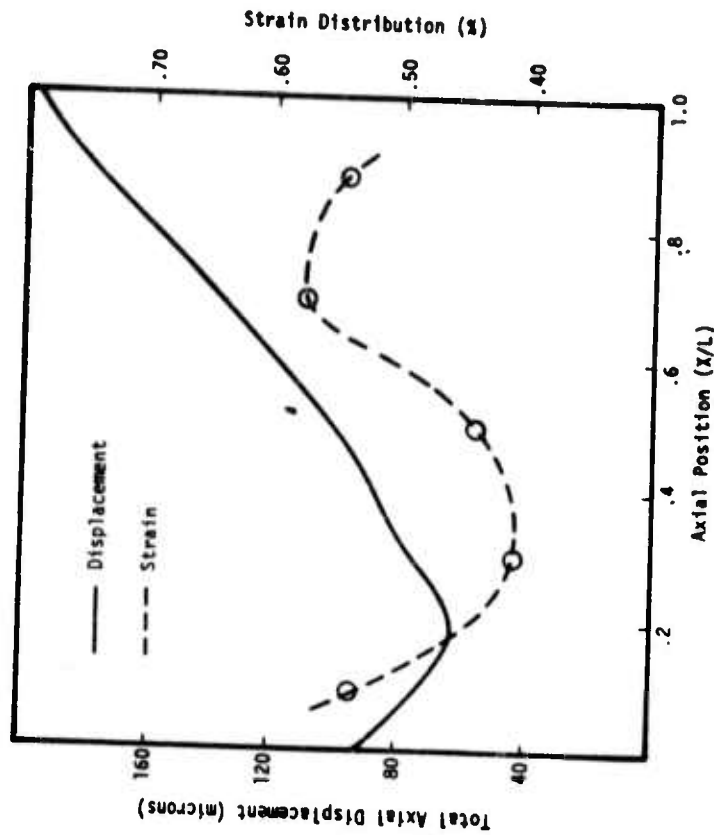
Figure 26B: Total axial displacement profile and strain distribution along axis for uniaxial test on Lithographic Limestone specimen. Total load increment 1000 psi to 5000 psi.
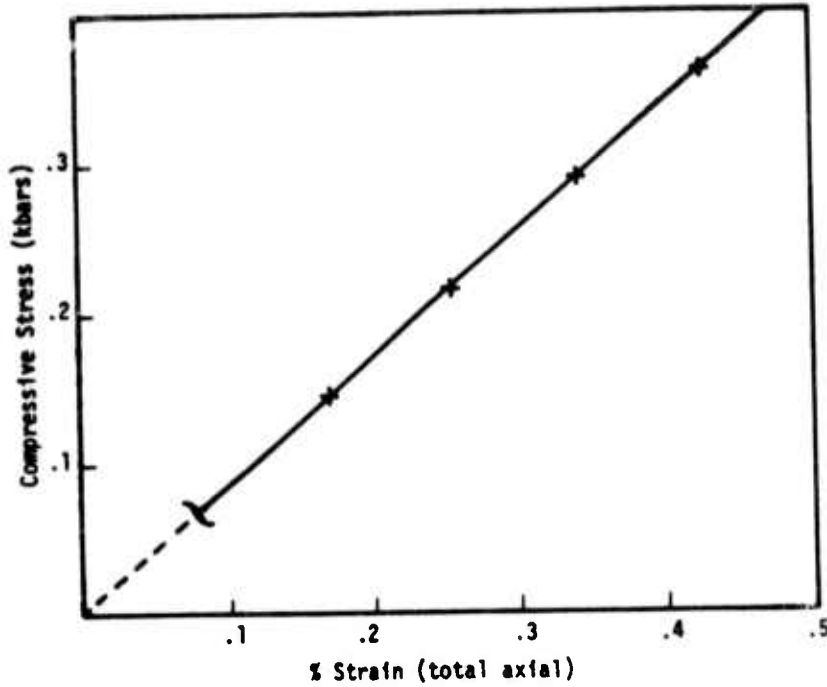
TRW.
SYSTEMS GROUP

Figure 27B: Total axial strain increments plotted against load increments for each interferogram for the uniaxial test on Lithographic Limestone.
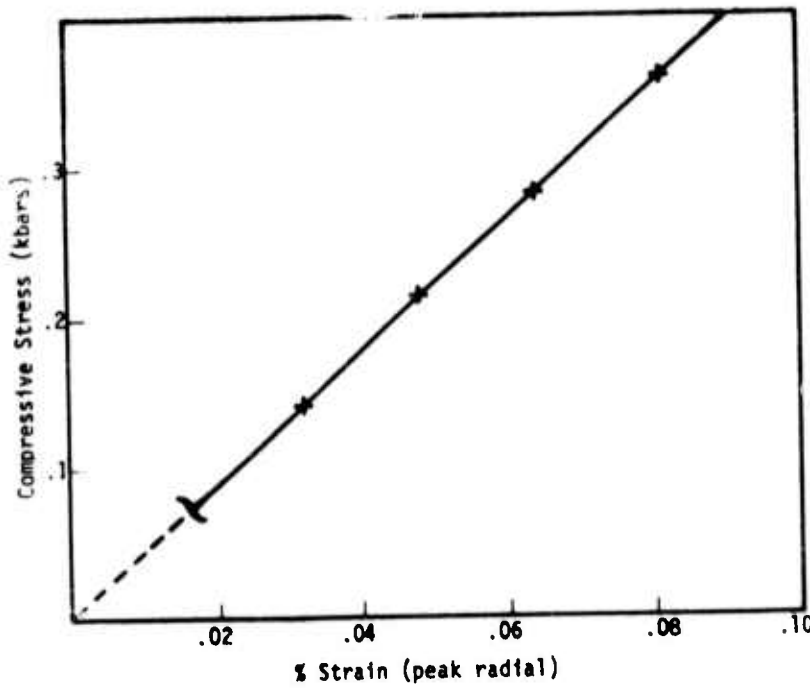
Figure 27A: Peak radial strain increments plotted against the load increments for each interferogram for the uniaxial test on Lithographic Limestone.

49

B   A

Figure 28: Photographs of holographic interferograms recorded during triaxial tests of Mixed Company Sandstone. The hydrostatic pressure was 4000 psi. In photo A the axial load was increased by 200 psi, in photo B 400 psi.

can be achieved (several kilobars) by using the synthetic sapphire windows in the form of cones and seated from the inside of the pressure vessel.

The problem with holography through the window could also be improved by using an antireflective coating on both sides of the window. This would eliminate the strong reflections off the front of the window which make it difficult to control the scene light intensities on the film and make it difficult to observe and photograph the fringes.

The data reduction for the triaxial test was carried out in the same manner as for the uniaxial tests in obtaining the radial and axial displacement profiles. It was necessary however to correct for changes in angles of viewing and incident light on the specimen due to ray refractions through the window and the pressurized water.

The radial displacement profiles for the two load steps are shown in Figure 29 A & B. The axial displacement profiles are shown in Figure 30 A & B. Again there was an uncertainty in the radial displacement profiles due to the correction of the absolute measurements for the estimated tilt of the specimen during the test. The ratio of the peak radial strain to the total axial strain for the test was .15. The total of radial displacements and axial displacements for the triaxial test are displayed in Figure 31 A & B.

The strain distribution along the viewing axis of the specimen is also shown along with the displacement profile. In both the uniaxial and the triaxial tests it can be seen that the compressive strain is not uniform over the length of the specimen as is assumed with conventional strain gauge measurements. Indeed there is a point where a high strain concentration is occurring and where the specimen is most likely to break. This was, in fact, demonstrated in previous uniaxial tests on Jasper Quartzite (Ref. 3) where the interferograms were taken of the specimen at loads near failure. Both the strain measurements and the fringe patterns in those tests predicted the region of failure initiation.
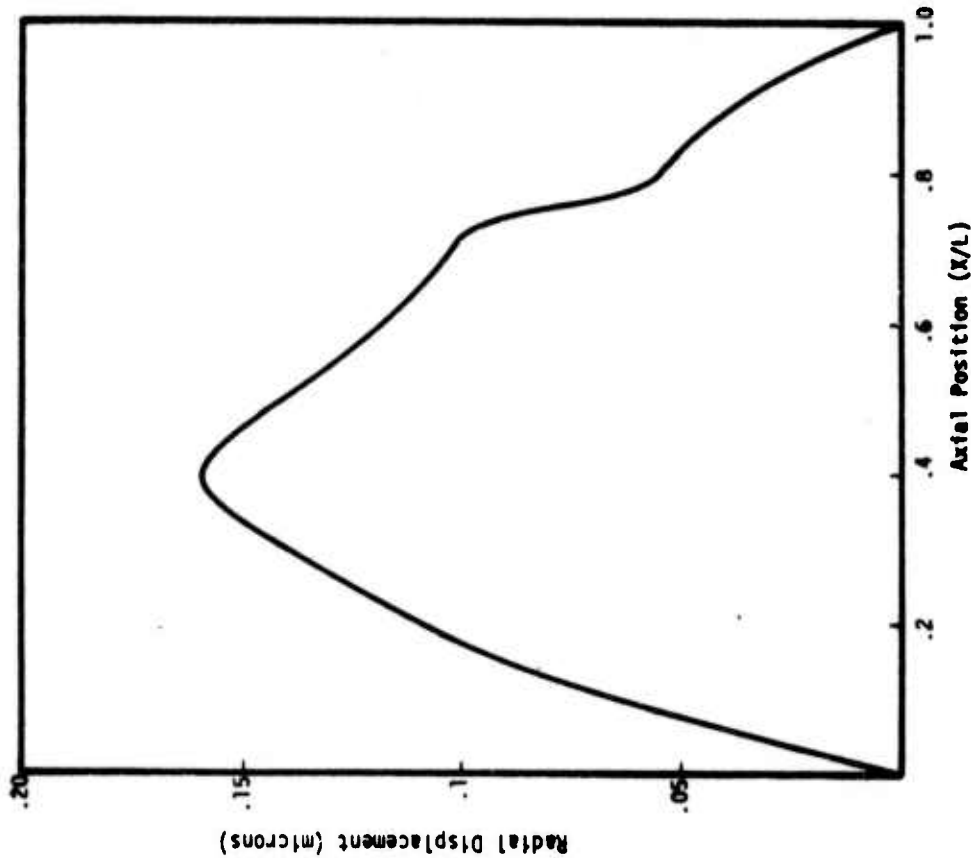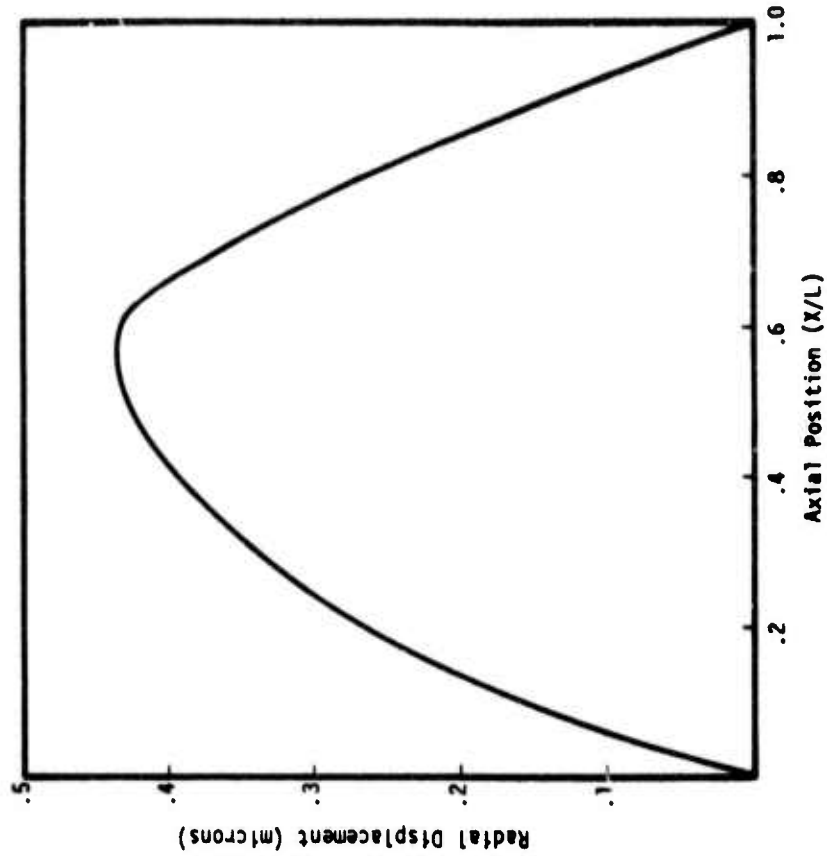
Figure 29A: Radial displacement profile along axis of triaxially loaded Mixed Company Sandstone specimen. $\sigma_3 = 4000$ psi. The axial load increment for the interferogram ($\sigma_1 - \sigma_3$) was approximately 250 psi.

Figure 29B: Radial displacement profile along axis of triaxially loaded Mixed Company Sandstone specimen. $\sigma_3 = 4000$ psi. The axial load increment for the interferogram ($\sigma_1 - \sigma_3$) was approximately 400 psi.
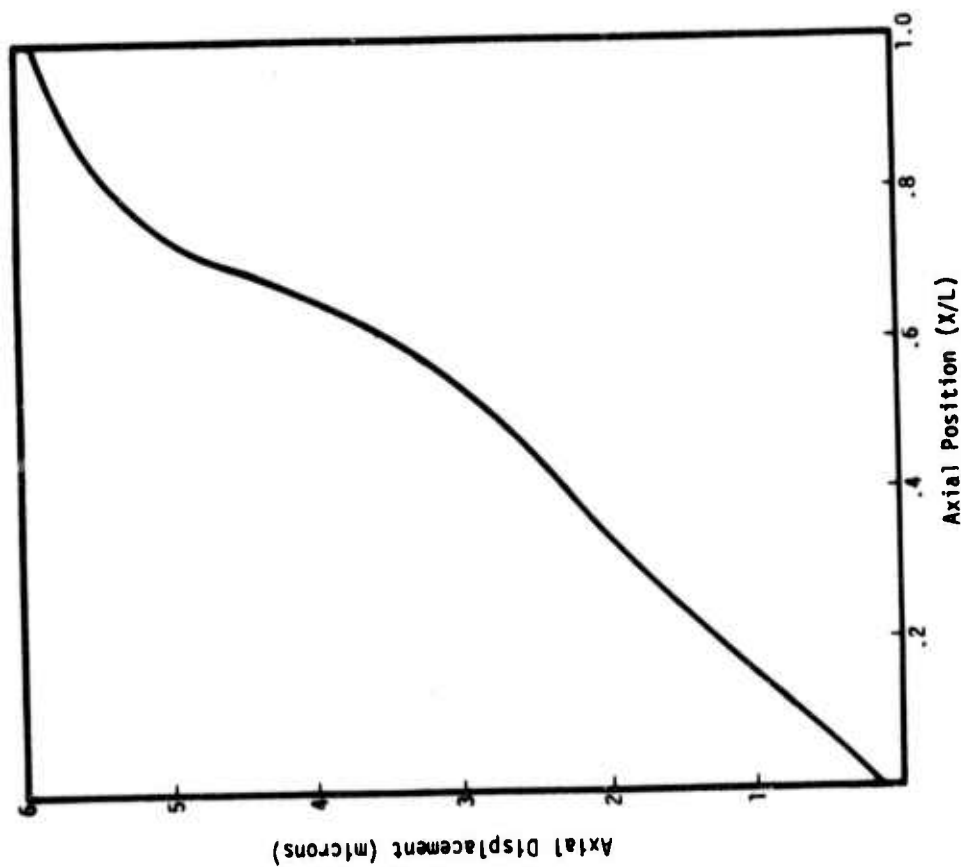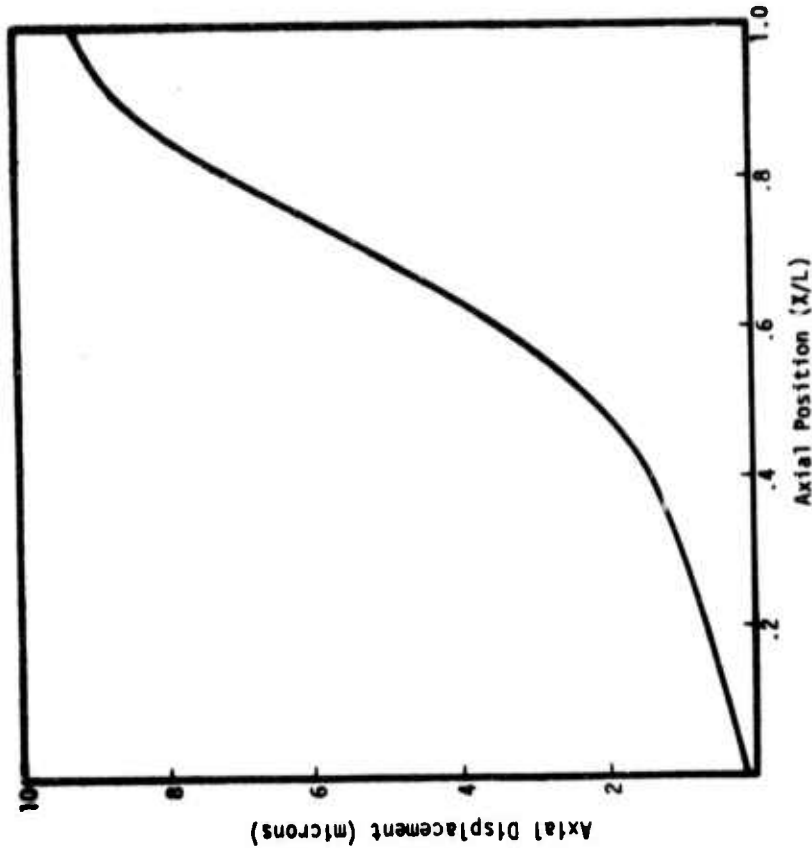
52

TRW
SYSTEMS GROUP

Figure 30B: Axial displacement profile along axis of the triaxially loaded Mixed Company Sandstone specimen. $\sigma_3 = 4000$ psi. The axial load increment for the interferogram $(\sigma_1 - \sigma_3)$ was approximately 400 psi.

Figure 30A: Axial displacement profile along axis of the triaxially loaded Mixed Company Sandstone specimen. $\sigma_3 = 4000$ psi. The axial load increment for the interferogram $(\sigma_1 - \sigma_3)$ was approximately 250 psi.
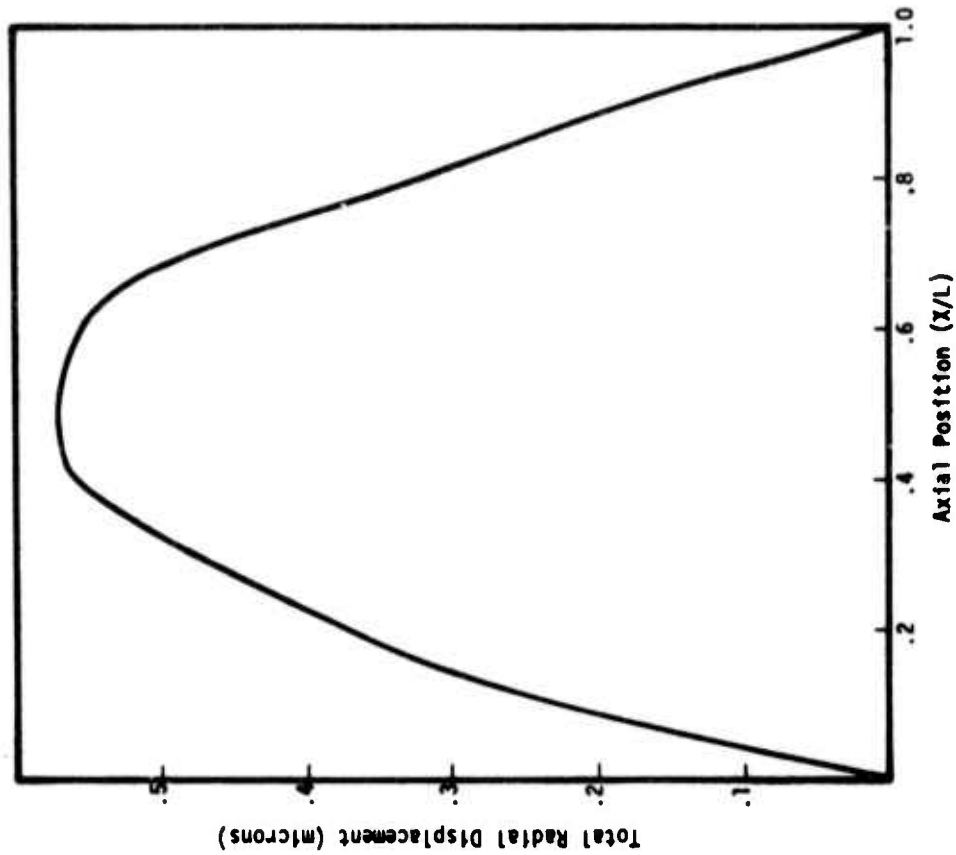
Figure 31B: The total radial displacement profile for the triaxial test of the Mixed Company Sandstone specimen. The hydrostatic pressure was 4000 psi. The total load range was approximately 1000 psi to 1650 psi.
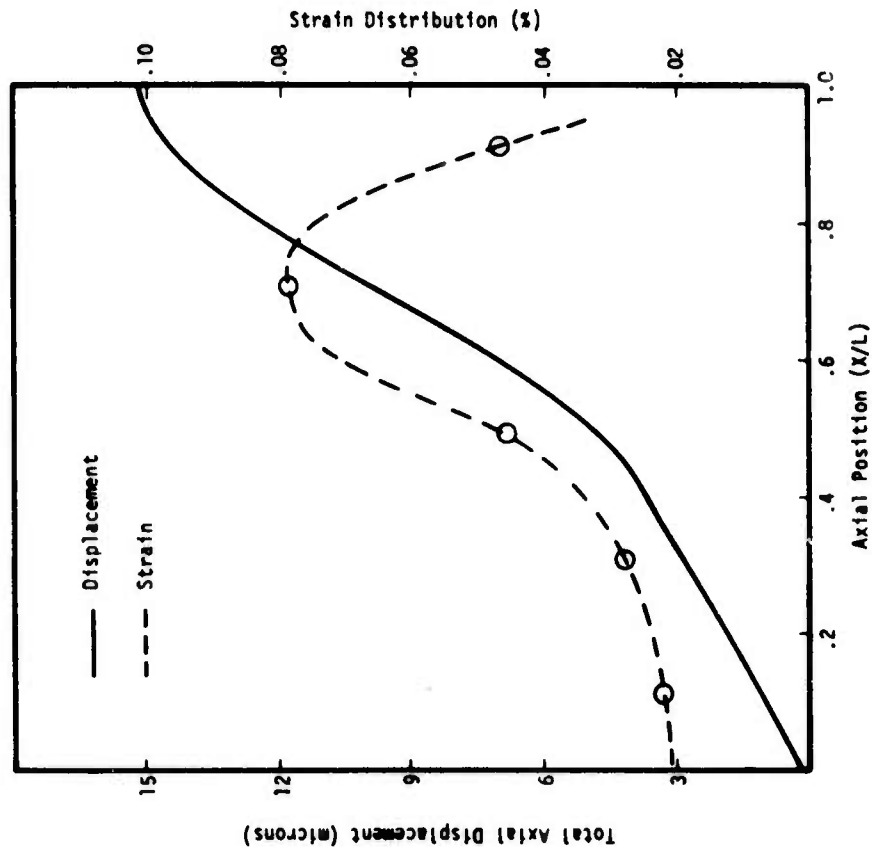

Figure 31A: The total axial displacement profile and strain distribution for the triaxial test of the Mixed Company Sandstone specimen. The hydrostatic pressure was 4000 psi. The total axial load range was approximately 1000 psi to 1650 psi.

TRW
SYSTEMS GROUP

5.0 REFERENCES

1. H. D. Stromberg and R. N. Schock, "A Window Configuration for High Pressure Optical Cells," Review of Scientific Instruments," December 1970.

2. R. Aprahamian and J. D. O'Keefe, "Experimental Investigation of Fracture of Granite Under Compression," TRW Systems Final Report, December 1971.

3. Dhir & Sikora, "Holographic Analysis of a General Displacement Field," Proceeding of the Symposium, Engineering Applications of Holography, February 1972.